



<http://waikato.researchgateway.ac.nz/>

Research Commons at the University of Waikato

Copyright Statement:

The digital copy of this thesis is protected by the Copyright Act 1994 (New Zealand).

The thesis may be consulted by you, provided you comply with the provisions of the Act and the following conditions of use:

- Any use you make of these documents or images must be for research or private study purposes only, and you may not make them available to any other person.
- Authors control the copyright of their thesis. You will recognise the author's right to be identified as the author of the thesis, and due acknowledgement will be made to the author where appropriate.
- You will obtain the author's permission before publishing any material from the thesis.

Characterisation, Consolidation and Mechanical Properties of TiAl Alloy Produced Using Titanox Powders



THE UNIVERSITY OF
WAIKATO
Te Whare Wānanga o Waikato

A thesis submitted in partial fulfilment
of the requirements for the degree of
Masters of Engineering
in Materials and Process Engineering

by

Bhupinder Singh Parmar

The University of Waikato, Hamilton, New Zealand
September 2007

Abstract

Characterization of the three different as-received TiAl powders, namely Tax1, Tax2 and Tax3 produced by Titanox development Ltd has been done. Predominate TiAl phase was observed in all the three compositions. The powder particles were very fine with average particle size of 12 μm , 5 μm and 10 μm respectively for Tax1, Tax2 and Tax3. Chemical analysis of the powders showed high oxygen content in all the three compositions of the powders.

Bulk samples were produced from Tax1, Tax2 and Tax3 powders by hot isostatic pressing at 1200° C under a pressure of 200Mpa for two hours. The pressurization gas used for the process was argon. The relative density of Tax1, Tax2 and Tax3 HIPped samples was 96%, 86% and 93% and respectively. The characterization of the HIPped samples showed that the predominate phase was γ -TiAl phase in all the three HIPped samples. A small fractions of Ti_3Al and TiAl_3 was also observed in tax1 and Tax3 HIPped material. Also some of the dark Al rich phases was Al_2O_3 phase in Tax1 and Tax3 HIPped samples. High oxygen content of the powder and air leaking in the can during the process of press-seal and welding of the end of the tube of the can prior to HIPping lead to poor consolidation of Tax2 which eventually resulted in high porosity and formation of Ti_2O and Al_2O_3 . Half of the Tax2 HIPped sample was canned and heated to 1160°C and was subjected to open die hammer forging with a high strain and a total reduction of height by 66%. The forging produced a pancake shaped sample without breaking of the sample.

Tensile specimens were cut from the Tax1 and Tax3 HIPped sample and one from the Tax2 forged sample using electrical discharge machine (EDM) wirecutting. Tax1 HIPped material showed the average fracture strength of 204MPa, 256MPa and 197MPa at room temperature, 800°C and 900°C respectively., Whereas Tax3 HIPped material showed average fracture strength of 103MPa and 234MPa respectively at room temperature and 800°C respectively. The HIPped and the forged Tax2 sample showed low fracture strength of 91MPa because of the micro-cracks produced during forging.

Acknowledgements

First of all I would like to thank my supervisor Associate Professor Deliang Zhang for giving me the opportunity to work on this project as a part of my M.E study, and for his enthusiastic and supportive supervision throughout the duration of my study. Special thanks to Dr. Brian Gabbitas and my company mentor Dr. Gorgees Adam for their valuable suggestions and ideas which I got from them time to time.

Thanks to the whole research team of the Department especially Vijay Nadakuduru, Stella Reynova, Aamir Mukhtar, Peng Cao, Asma Salman and Masleeyati Yusop for the help and the support. Thanks to Paul Ewart, Yuanji Zhang, Inder Singh, and Helen Turner for their technical support and assistance.

I would like to thank the New Zealand Foundation of Research, Science and Technology for funding this project through Technology for Industry Fellowship (TIF Contract no: TTXX0601).

Table of Contents

Abstract	iii
Acknowledgements	iv
Table of Contents	v
List of figures	vi
List of Tables	viii

Chapter One **Introduction and Literature Review**1

1.1 Introduction	02
1.2 Properties, Applications and Limitations of the Titanium Alloys.....	03
1.3 Titanium Aluminide Based Alloys and Their Properties and Applications.....	05
1.4 The effects of Microstructures on the Properties of TiAl Based Alloys.....	10
1.5 Effects of Compositions.....	13
1.6 Processing of TiAl Based alloys.....	14
1.6.1 Reaction Sintering.....	15
1.6.2 Hot Pressing.....	16
1.6.3 Spark Plasma Sintering.....	17
1.6.4 Hot Isostatic Pressing	18
1.6.5 Equal Channel Angular pressing/extrusion.....	21
1.7 Secondary processing.....	21
References.....	23

Chapter Two **Experimental Procedure**28

2.1 Powder Compaction.....	29
2.2 Degassing and Canning of the powder Compacts.....	30
2.3 Powder Consolidation by Hot Isostatic Pressing.....	32
2.4 Secondary Processing of the Consolidated Sample.....	33
2.5 Tensile Specimen Preparation.....	34
2.6 Mechanical Testing.....	34
2.7 X-Ray Diffractrometry.....	34
2.8 Density Measurement.....	35
2.9 Microscopy and Particle Size Analysis	35
2.10 Microhardness Testing.....	36

Chapter Three **Results and Discussions**.....37

3.1 Powder Characterization.....	38
3.2 Consolidation Behaviour of the Titanox Powders in Hot Isostatic Pressing.....	45
3.3 Microstructures of the Hipped Samples Produced Using Titanox Powders.....	48
3.4 Mechanical Behaviour of Hipped Samples Produced Using Titanox Powders	54
3.5 Forging of the Tax2 Hipped Sample.....	58
3.6 Fracture Behaviour of the Tensile Testing Specimens	63
3.7 Discussion.....	65
References.....	67

List of Figures

Figure. 1.1: (a) Specific modulus and (b) specific strength of different materials as a function of temperature	06
Figure 1.2: Some of the application of TiAl based alloys in HSCT:	
(a) Boxed area, Exhaust nozzle Engine of HSCT propulsion System (b) the use of TiAl for major nozzle component (c) TiAl Honey Comb panel	07
Figure 1.3: TiAl Turbocharger turbines	
	08
Figure-1.4: DO ₁₉ structure of Ti ₃ Al, (Ti-A, Al-B)	
	09
Figure-1.5: L1 ₀ structure of TiAl, (Ti-A, Al-B)	
	09
Figure 1.6: Ti-Al Phase Diagram	
	10
Figure 1.7: Different types of microstructures of TiAl based alloys	
	11
Figure 1.8: Grain size (d) and lamellar width (λ) for polycrystalline TiAl alloys with a fully lamellar microstructure	
	12
Figure1.9: Schematic diagram of hot pressing furnace used for consolidation powders	
	16
Figure 1.10: Schematic diagram of the set-up of spark plasma sintering	
	18
Figure 1.11: Schematic diagram of the set-up of a Hot Isostatic press vessel	
	20
Figure 1.12: Examples of TiAl based prototype components produced by forging:	
(a) Turbine blade (b) shroud part of the turbine and (c) half of top cone of turbine	22
Figure 2.1: Cold Isostatic press used in compacting the powder	
	29
Figure 2.2: Canned sample before de-gassing and sealing	
	30
Figure2.3: The Pressing die and the fixture used for press-sealing the tube	
	31
Figure 2.4: Sealed cans after de-gassing and press-sealing and welding	
	31
Figure 2.5: Hot Isostatic Press	
	32
Figure 2.6: Graphical representation of temperature and pressure change during the HIPping process	
	33
Figure 2.7: (a) Hipped Tax2 concealed by stainless steel can before Forging (b) Side view of the disk produced by forging of the consolidated sample and (c) Planar view of the disk which a tensile test specimen being cut from the disk	
	33
Figure 2.8: (a) Tensile specimen from Hipped sample (b) tensile specimen from forged sample	
	34

Figure 3.1: Powder particle morphology and size of the as received Titanox powders (a) Tax1powder (b) Tax2 powder (c) Tax3 powder	39
Figure 3.2: Normalised powder particle size distributions for the powders	40
Figure 3.3: XRD Patterns and analysis of the as-received Titanox Powders	40
Figure 3.4: (a) Cross section of the particles in the Tax1 powder (b) EDS spectrum from the point shown by the cross in (a)	41
Figure 3.5: (a) Cross section of the particles in the Tax2 powder (b) EDS spectrum from the point shown by cross in (a)	42
Figure 3.6: (a) Cross section of the particles in the Tax3 powder (b) EDS spectrum from the point shown by cross in (a)	43
Figure 3.7: Consolidated samples produced by hot isostatic pressing of Titanox powders: (a) Tax1 (b) Tax2 (c) Tax3	46
Figure 3.8: Optical micrograph of the hipped samples produced using Titanox powders (a) Tax 1(b) Tax2 (c) Tax3	47
Figure 3.9: XRD Patterns of the consolidated samples produced by HIPping Titanox Powders Hipped at 1200 °C	48
Figure 3.10: (a)SEM secondary electron image of Tax1 HIPped sample; (b) EDS spectra from points 1-3 shown on the image respectively	50
Figure 3.11: (a) SEM image and (b) and (c)X-ray elemental maps of Tax1 Hipped sample	51
Figure 3.12: (a) SEM secondary electron image of the microstructure of Tax3 HIPPed sample and (b) EDS spectra from points 1-3 shown on the image respectively	52
Figure 3.13: Stress vs Strain curves of specimens from Tax1 HIPped sample tested at room temperature	55
Figure 3.14: Broken Tensile specimens of Tax1 tested at room temperature (a) specimen 1 (b) specimen 2	55
Figure 3.15: Stress vs Strain curves of specimens from Tax1 HIPped sample tested at 800 ° C	56
Figure3.16: Stress vs Strain curves of specimen from Tax1 HIPped sample tested at 900° C	56
Figure 3.17: Stress vs Strain curves of a specimen from Tax3 HIPped sample tested at room temperature	57

Figure 3.18: Stress vs Strain curves of specimens from Tax3 HIPped sample tested at 800° C	57
Figure 3.19: (a) Hipped Tax2 concealed by stainless steel can before Forging (b) Side view of the disk produced by forging of the consolidated sample (c) Planar view of the disk	59
Figure 3.20: Optical micrograph of Tax2 (a) Hipped at 1200°C (a) Hipped and Forged at 1200°C	59
Figure 3.21: Cracks on the tensile specimen cut from the forged disk	60
Figure 3.22: XRD Patterns of Tax2 Hipped sample before and after and Forging	60
Figure 3.23: SEM secondary electron image of Tax2 HIPped sample after forging	61
Figure 3.24: : (a) SEM secondary image of Tax2 HIPped sample after hot forging(b)EDS spectra from point 1-3 shown in (a) respectively	62
Figure 3.25: Broken Tensile specimens for Tax1 tested at (a) Room temperature (b) 800° C and (c) 900°C	63
Figure 3.26: SEM secondary electron images of the fractured surface of tensile testing specimen for Tax1 HIPped sample tested at room temperature	64
Figure 3.27: SEM secondary electron images of the fractured surface of tensile testing specimen for Tax1 HIPped sample tested at 800°C	64
Figure 3.28: SEM secondary electron images of the fractured surface of tensile testing specimen for Tax1 HIPped sample tested at 900°C	64

List of Tables

Table 1.1 Shows some of the properties of Titanium Aluminide Alloys	05
Table 3.1: Content (in at%) of different elements in the threes particles shown in Figure 3.4-3.6 determined using semi-quantitative EDS analysis	44
Table 3.2: Concentration of different elements in different phases determined using semi-quantitative EDS analysis of Tax1 hipped sample	51
Table 3.3: Concentration of different elements in different phases determined using semi-quantitative EDS analysis of Tax3 hipped sample	53
Table 3.4: Fracture strength of Tax1 and Tax3 HIPped samples at different temperatures	58

CHAPTER ONE:

Introduction

and

Literature Review

1.1 INTRODUCTION

We have entered the Titanium era with the commencement of the 21st century. With the specific gravity of 4.54g/cm³, titanium and titanium alloys have become materials of great technological importance. Titanium is not actually a rare element and it stands fourth most abundant metallic element in the earth's crust and comes after aluminium, iron and magnesium [1]. Unfortunately it is not found in high concentration and real state and its extraction is not easy an job because of the high processing costs.. Despite this fact, titanium alloys and titanium based intermetallics like TiAl, Ti₃Al are gaining more importance worldwide because of their favourable properties such as high strength to weight ratio, excellent corrosion resistance, creep resistance and thermal stability of microstructure.

They are considered to be potential candidates for the structural materials and has big room for the advancement in many fields like aerospace and other terrestrial applications where weight to thrust ratio is the key. [1-3]. Where weight is an issue TiAl based alloys can be potential replacement to heavy nickel base alloys and super alloys which shows excellent elevated temperature properties [3]. Room temperature ductility and oxidation at higher temperatures are the main hurdles slackening the progress of these alloys [3,4]. Properties of the TiAl based alloys mainly depends upon the alloying elements and the microstructures , so most research done to these materials is basically to optimize microstructure so that optimum balance of the properties can be achieved.

The present thesis presents and discusses a study on the results of the characterization of three TiAl based powders of similar compositions produced by Titanox Development Ltd. and on the quality, microstructure and mechanical properties of the consolidated TiAl based alloys, produced by hot isostatic pressing (HIP) of the three Titanox powders. One of the HIPped samples was also subject to forging, and the microstructure of the HIPped and forged sample was also studied. The objectives of the study are:

- To gain a good understanding of the characteristics such as particle size distribution, particle morphology, microstructure and compatibility of the Titanox TiAl powders.

- To study the microstructure and mechanical properties of the consolidated material produced by hot isostatic pressing of Titanox powders so that their future potential applications can be predicted.
- To compare the microstructure and mechanical properties of the HIPped material produced from the three Titanox powders.

The present chapter first gives the introduction and a brief description of titanium alloys, their applications and their limitations. It then presents a literature review on the TiAl based alloys, covering their processing, different microstructures and the influence of microstructure on the mechanical properties.

1.2 Properties, Applications and Limitations of the Titanium Alloys

High specific strength to ductility ratio and excellent corrosion are the two important properties which make titanium alloys preferential candidates for the use in aerospace, chemical engineering and bio-medical engineering and sports good industries. At low temperatures ($<882^{\circ}\text{C}$) pure titanium has a hexagonal close packed structure and is called α titanium. At higher temperatures ($>882^{\circ}\text{C}$) pure titanium is transferred to β phase which has a body centred cubic crystal structure (bcc) [6]. Alloying elements of titanium are classified as neutral, α stabilizers and β stabilizers depending on their influence on the α/β transus temperature. The α stabilizing elements (Al, O, N, and C) extends the α phase field to higher temperatures, while β stabilizers (Cr, Mn, V, Mo, and Nb) extends the β phase field to lower temperatures. Usually titanium alloys are classified as α , $\alpha + \beta$, and β alloys with further subdivision into near α and metastable β alloys[6,7] The α alloys mainly comprise of commercially pure (CP) titanium and the alloys with α - stabilizing elements and /or neutral elements. At room temperature these alloys mainly consist of α - phase. If a very small amount of β - stabilizing elements are added to the α alloys .If a substantial amount of β stabilizing alloys are added to α alloys , α/β alloys are formed and at room temperature alloys have of 5 - 40% vol. of β phase. If a titanium alloy contains little or no α stabilizing elements and the content of β stabilizing elements is increased to a stage where β does not transform to martensite upon fast quenching α/β or metastable β alloy is formed.

Basically the size, morphology, volume fraction and the individual properties of the two phases α phase and β phase are the parameters which determine the mechanical properties of titanium alloys. The α phase has an anisotropic hcp crystal structure which is more densely packed as compared to bcc crystal structure of the β phase. Compared with β alloys, α and α/β alloys have higher resistance to plastic deformation, higher creep resistance, reduced ductility, and anisotropic mechanical and physical properties and are primarily used in chemical and process industry. Ti-6wt%-Al 4wt %V (Ti-6-4) alloy is the classic example of α/β alloys and it is most widely used titanium alloy. It has high specific strength, weldability, good corrosion resistance and good biocompatibility to human tissue. [8].

β titanium alloys are the most versatile class of titanium alloys. Ti-13wt%V-11wt %Cr-3wt%Al (Ti-13-11-3) alloy was the first significant β -alloys developed . It was extensively used on the SR-71 “blackbird” airplane. One of the reasons for the selection for Ti-13-11-3 was its thermal stability and was used for wing and body skins, frames, longerons, ribs and the main and the nose landing gears [8,9].

However, the mechanical strength and creep behaviour of titanium alloys become inadequate for operating temperatures over 500° C. Moreover oxidation problems also arise because of the formation of oxide, nitride and /or hydride layer at their surface which leads to embrittlement and thus premature fracture and damage [3]. After an intensive research period of about 15 years gamma titanium (γ -TiAl) based alloys have been successfully developed [1]. γ -TiAl alloys are light weight, high strength materials thought to be capable of operating at temperatures up to 1000°C which is just below the temperatures where ceramics are commonly used making them in just below the temperatures where ceramics are commonly used making them ideal for making components for high temperature applications. Because of this special attribute, TiAl based alloys have attracted strong research and development interests of research organizations and industrial companies [10].

1.3 Titanium Aluminide Based Alloys and Their Properties and Applications

Titanium aluminides are the intermetallics which have mechanical properties lying somewhere between ceramics and metallic alloys [11]. Their characteristics such as high temperature stability, good strength and stiffness at high temperatures, low density, good oxidation resistance, good deformability at high temperatures make this type of materials valuable and potential candidates for high temperature structural materials. Demands for the design requirements pertaining to energy conservation systems with improved efficiency and ecological compatibility are ever increasing. Titanium aluminides alloys based on the intermetallics phases' γ (TiAl) and α_2 ($Ti_3 Al$) have the potential to meet these design requirements. Table 1.1 shows some of the properties of two widely studied titanium aluminides TiAl and $Ti_3 Al$ alloys [11]. Properties like specific modulus and strength of TiAl based alloys are remarkably higher than that of alloy steel and nickel based alloys specially at high temperatures (Figure 1.1).

Table 1.1 Some of the properties of Titanium Aluminides Alloys [11]

Titanium Aluminide Alloys	TiAl	$Ti_3 Al$
Density(g/cm ³)	3.8	4.2
E(GPa)	160-180	100-150
YS(MPa)	400-650	700-1000
Fracture toughness(MPa m ^{1/2})	10-20	10-20
Temperature limit due to creep(° C)	800-900	750
Temperature limit due to oxidation(° C)	800-900	650

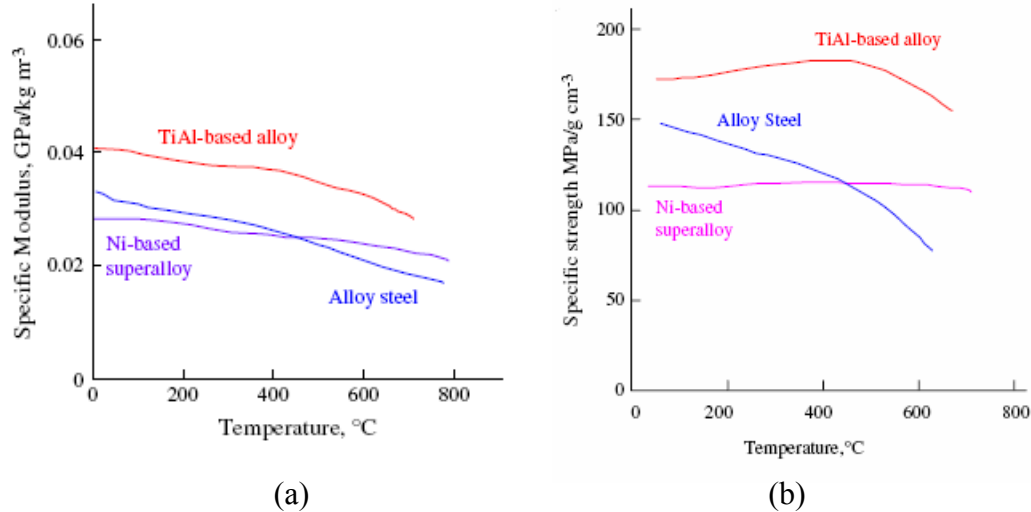


Figure. 1.1: (a) Specific modulus and (b) specific strength of different materials as a function of temperature[12]

Because of these unique properties, TiAl based alloys have great potential for aerospace and terrestrial applications. High speed civil transport (HSCT) is a second generation super sonic commercial aircraft which is being developed by NASA whose objective is to meet the increasing overseas travel demand. TiAl honey comb panels are being considered in the Reusable launch vehicle program 1.2(c).Also TiAl based alloys found rooms in the fabrication of several critical components for the exhaust nozzle in the vehicle. Cast TiAl was selected for the divergent flap of the nozzle whereas cast sheet was used as side wall Figure 1.2(a) and (b)[13].

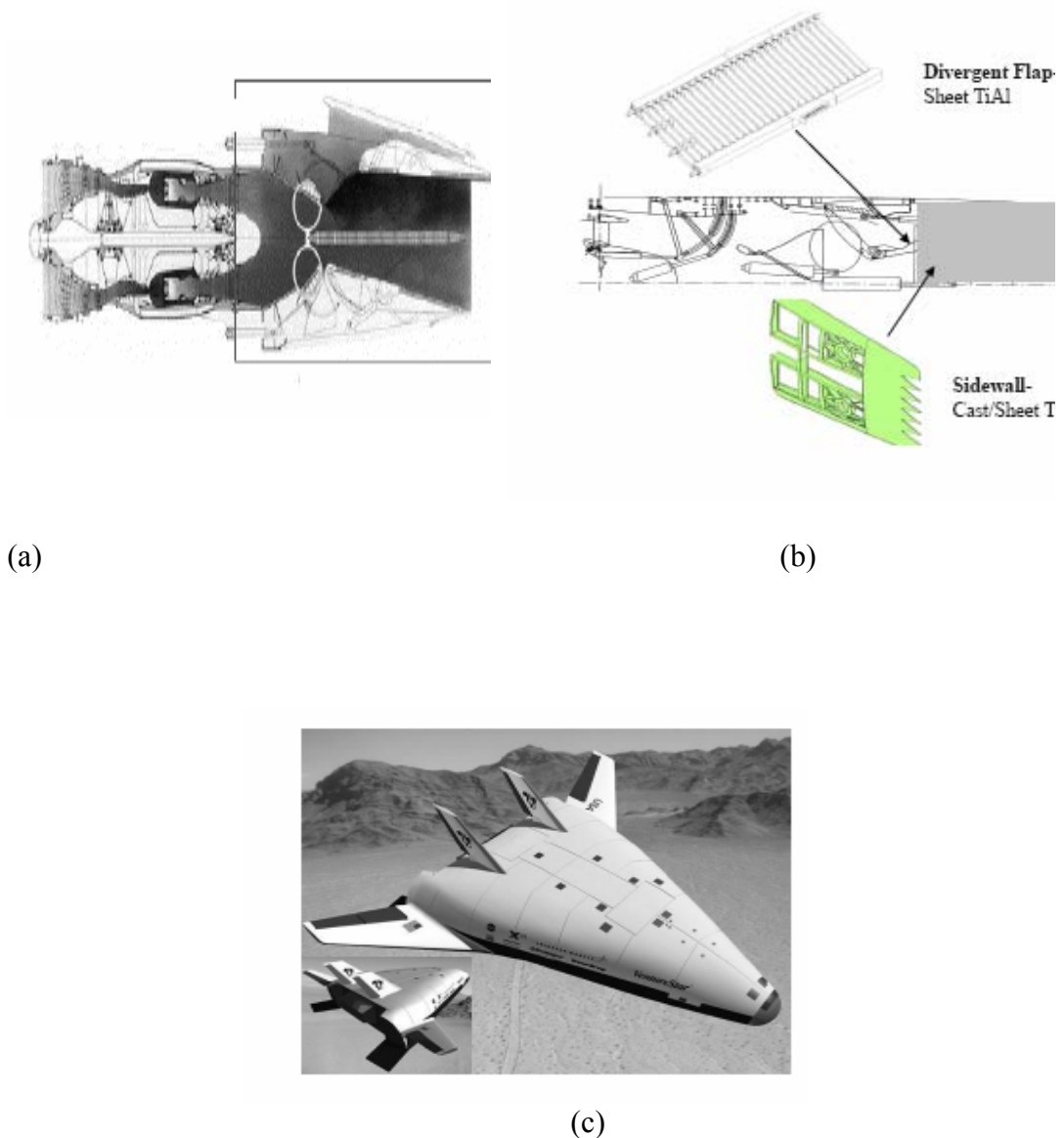


Figure 1.2 Some of the application of TiAl based alloys in HSCT: (a) Boxed area, Exhaust nozzle Engine of HSCT – propulsion System (b) the use of TiAl for major nozzle component (c) TiAl Honey Comb panel [13]

Turbocharger (Figure 1.3) made of TiAl alloy containing niobium being used for commercial cars of special type turbines. Such turbines operate at temperatures up to 1000° C without any surface coating. [16].

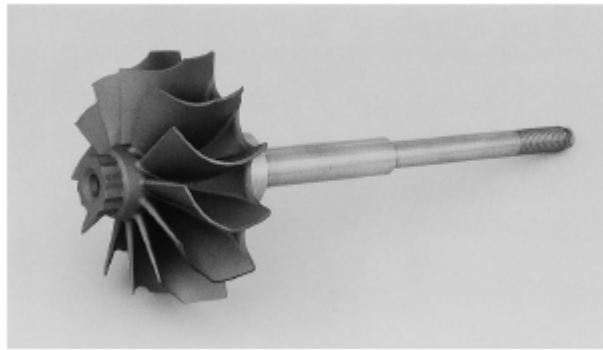


Figure 1.3: TiAl Turbocharger turbines[16]

The exceptional thermo-physical properties of TiAl based alloys depend on the strongly ordered nature and directional bonding of the compounds. The highly ordered crystal structure and strong directional bonding accounts for the high specific strength of titanium aluminide alloys at high temperature [11]. α_2 - (Ti_3Al) is an ordered phase with hexagonal DO_{19} structure (Figure1.4). It has limited ductility at room temperature and improves at higher temperature. Addition of small percentage of β stabilizer like niobium of about 4% increases the ductility. Ti-25Al-10Nb-3V1-1Mo is an example of alloys based on α_2 . γ (TiAl) has a face centered tetragonal $L1_0$ ordered structure (Figure-1.5), melts at about $1460^{\circ}C$ and again, it shows good oxidation resistance ,good thermal stability, higher stiffness and slightly lower strength than that of Ti_3Al .

TiAl based alloys have compositions of 42-47at.% Al with other alloying additions like manganese and niobium for ductility and high temperature capability [13]. One of the examples is Ti-42at%Al – (1-10) at % (Cr, V, Mn, Nb, Mo, and W) Cr, Mn, V and Si increase ductility but decrease oxidation resistance while additions of Mo, W, and Nb increase oxidation resistance and Si, C and N in small amounts are good for the creep resistance [6].

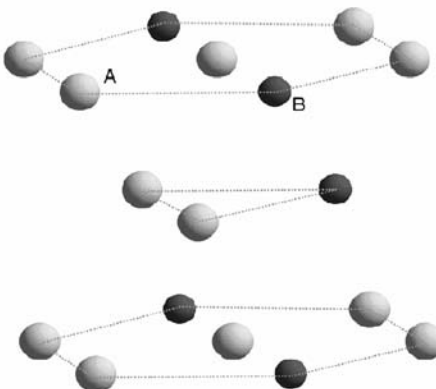


Figure-1.4: DO_{19} structure of Ti_3Al , (Ti-A, Al-B) [12,13]

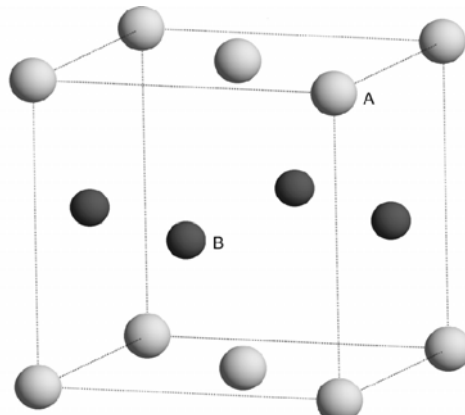


Figure-1.5 : $\text{L}1_0$ structure of TiAl , (Ti-A, Al-B) [12,13]

As shown in the Ti-Al binary phase diagram (Figure 1.6) during cooling of Ti-Al alloy liquid with a composition of 42-47wt% Al. The liquid generally starts solidifying with formation of β phase and goes through peritectic reaction with the formation of $\text{L} + \beta \rightarrow \alpha$. On further cooling the α turns into a mixture of α and γ [6,[14,15]. γ TiAl can solidify in a single phase state only when the aluminium content exceeds about 53 at.%. through a peritectic reaction $\text{L} + \alpha \rightarrow \gamma$. Single phase γ TiAl alloys suffers from poor ductility and poor fracture toughness. Considerable ductility and toughness can be achieved in two phase γ alloys with composites consisting of α and γ phases. Generally research is carried out to develop two phase structure consisting of γ - TiAl phase and α_2 - Ti_3Al phase [15]

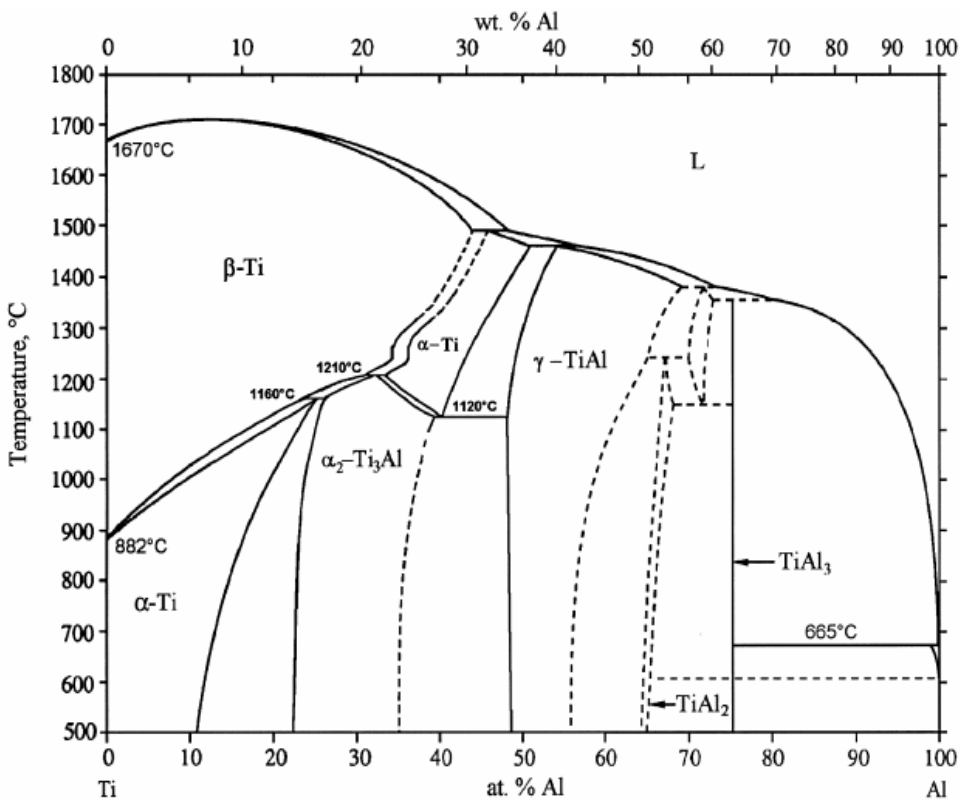


Figure 1.6 Ti-Al Phase Diagram [15]

1.4 The effects of Microstructures on the Properties of TiAl Based Alloys

Mechanical properties of the TiAl based alloys strongly depend on the microstructure. Therefore, by controlling the microstructure, the required mechanical properties can be obtained to meet the needs for a specific component. In order to achieve uniform properties especially in complex shaped components thorough knowledge of properties/microstructure relationship becomes extremely important [15,17].

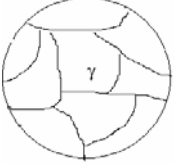
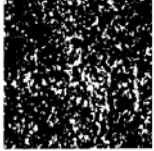
 (a)	Single γ: Equiaxed γ grains
  (b)	Duplex: Equiaxed γ grains and lamellar grains with small α_2
  (c)	Fully lamellar: Equiaxed lamellar grains of alternating γ and α_2 Platelets

Figure 1.7: Different types of microstructures of TiAl based alloys
[11, 15, 19]

Generally TiAl based alloys are processed to obtain one of the three major types of microstructures. One type of microstructure consists of only equiaxed γ grains (Figure 1.7(a)). The second type of microstructure consists of duplex microstructure which consists of equiaxed grains of γ phase and lamellar grains alternating layer of γ and α_2 platelets (Figure 1.7(b)). The third type of microstructure is a fully lamellar consisting of alternating of γ and α_2 platelets (Figure 1.7(c)) [14, 17]. The volume fraction of the lamellar grains increases in the following order; single γ microstructure, duplex microstructure, fully lamellar microstructure.

Fine and homogeneous duplex microstructure results in good ductility where as lamellar structure are poor in ductility but are superior in other properties such as fracture toughness, fatigue resistance and high temperature creep resistance. TiAl based alloys with microstructure consisting of fine equiaxed γ –TiAl grains and a small fraction of lamellar colonies show moderate tensile ductility and strength at room temperature and elevated temperature but comparatively they show substantially lower fracture toughness and creep resistance at high temperature [14, 15].

The microstructural design of the TiAl based alloys should be such that the properties like ductility, toughness and creep resistance has to be optimum for given applications. Overall balance of these properties is comparatively better in TiAl based alloys with a fully lamellar microstructure than those with duplex or near gamma microstructure.[19,20] The microstructure of fully lamellar TiAl alloys is generally characterized by the lamellar spacing or width λ , and grain size d as schematically shown in Figure 1.8 [16]

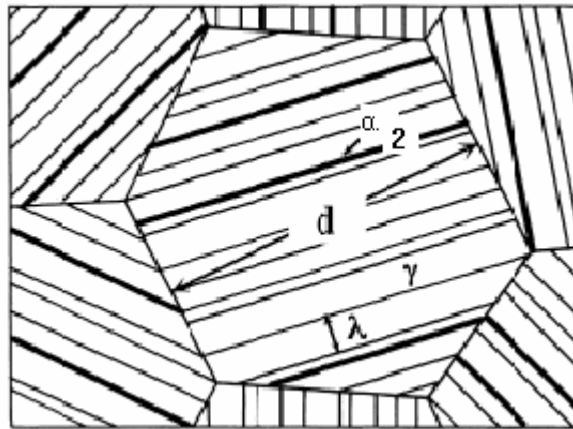


Figure 1.8: Grain size (d) and lamellar width (λ) for polycrystalline TiAl alloys with a fully lamellar microstructure [16]

The tensile strength of TiAl based alloys increase with decreasing grain size generally following the typical Hall-pitch relationship. While considering the creep resistance, the influence of the lamellar spacing is more obvious than that of grain size. Creep resistance increases with the decreasing lamellar spacing in fully lamellar TiAl alloys [21, 22]. Decreasing lamellar spacing decreases the creep rate, which is more noticeable at higher temperature [22]. The fatigue crack growth rate of TiAl based alloys is another important property for its application which is also sensitive to its microstructure. Lamellar structure shows the highest crack growth resistance and the duplex structures were better than equiaxed grain structure [24].

1.5 Effects of Compositions

Composition is an important parameter on which properties of TiAl based alloys strongly depend. In other words, properties of TiAl based alloys are very sensitive to their chemical compositions and even a small change in the compositions can change the properties significantly [7,24]. Change in Al contents effects more than that of other alloying elements because of the aluminium induced changes in the microstructure. In the meantime oxidation rate increases appreciably with the decrease of Al content from 50 at% to 48at% at 900°C [16].

Alloying element addition exists in either interstitial or substitutional form in TiAl. They not only modify the phase equilibrium and inherent electron bonding but also affect the stacking fault energy, resistance to dislocation modes, anti-phase boundary [APB] energy and the twin boundary energy. Addition of transition elements with high melting point increases the high temperature strength, so do the non metallic elements like nitrogen, carbon and silicon because of solid solution and precipitation hardening [16]. TiAl doped with carbon hardens appreciably by the precipitation of carbides. Also fine precipitation of carbides results in the increase in high temperature strength and remarkably decreases the grain size [25].

Boron or combination of boron and transition metals refines the grains and also stabilize the lamellar structure provided that the titanium boride particles formed are fine. Large titanium boride particles are detrimental to the tensile ductility [3,16,27]. Titanium boride particle acts as a barrier for grain growth at high temperatures. Addition of up to 10%at of Nb improves the oxidation resistance of TiAl based alloys as it suppresses the rutile growth and helps to form a thick continuous outer layer of Al_2O_3 seal and also it improves the resistance to environmental attacks. However, this improvement of the oxidation resistance is at the expense of the ductility. Even 1at.% of Nb added to TiAl based alloys leads to a decrease of elongation of fracture by 1% [28]. Addition of Cr of up to 2at% acts as beta stabilizer and improves ductility. However for binary alloys properties strength depends mainly on microstructure .Addition of small amounts of

Chapter 1: Introduction and Literature Review

chromium leads to fewer lamellar grains and more γ -grains. The microstructure can thus be deformed without hindrances induced by harder α_2 phase.

Previous research shows that slight improvement regarding brittleness of TiAl compound by means of alloys modification. However there is more room for improvement by changing the microstructure through various heat treatment processes. For example, Zhang's group at Central Iron and Steel Research Institute China developed a type of alloy Tac-1(Ti-46.5Al-2.5V-1Cr in at%)and showed that fine fully lamellar microstructure can be obtained by the application of series of heat treatment .This fine fully lamellar structure shows better combination of fracture toughness(20MPa \sqrt{m}) and ductility(~3.5%) at room temperature [29].

1.6 Processing of TiAl based alloys

Several processes can be used to manufacture components out of TiAl based alloys .TiAl based alloys are normally made using Ti and Al metals and other alloying metals in the form of elemental metals or master alloys by plasma arc melting, induction melting or vacuum arc melting, casting, powder metallurgy, forging and sheet metal forming. Conventional forging methods are associated with high production cost and also difficulty in shaping [30]. Casting was thus believed to be most cost effective process a decade ago. Also casting gives good high temperature strength due to large grain and cast texture which makes it suitable for making turbine blades. But cast products suffer from cast defects and chemical inhomogeneities [18]. Cast products are associated with high porosity level, easy cracking at high stress concentration, anisotropic property behaviour and are difficult to repair. Since this study is concerned with the use of powder metallurgy to make TiAl based alloy samples , the review on processing of TiAl based alloy is focussed on powder metallurgy and secondary processing of TiAl alloys produced using powder metallurgy.

Powder metallurgy is considered to be an effective approach in shaping TiAl based alloys. It gives better microstructural and chemical homogeneity and offers potential to make near net shaped component combined with mechanical properties that are equal or exceed cast and wrought products. Texture free

materials can be obtained with fine uniform grain structures plus good chemical homogeneity with substantially reduced machining waste and scrap rate [36]. Basically powder metallurgy consists of producing fine powders, mixing and making the powder for future use, pressing the powder into the desired shape, sintering the powder compact at an elevated temperature. Powder production again can be done by direct reduction from oxides, electrolytic deposition or it can be by atomisation of liquid metals. The green compact formed after the powder compaction is consolidated using appropriate consolidation process to make the TiAl parts. These processes include pressure less sintering, hot pressing [36], reactive sintering [36,37], hot isostatic pressing[34,35], equal channel angular pressing or Extrusion (ECAP/ECAE) and extrusion in each of the major processes . In the following subsection research work published in literature is reviewed.

1.6.1 Reaction Sintering

Reaction sintering, also called combustion synthesis or self propagating high temperature sintering, has received considerable attention for the last couple of decades. This is an innovative method and is employed to fabricate ceramics, intermetallics and metallic (or, intermetallic)-ceramic in-situ composites [33,36]. This method avoids the use of prolonged high temperature treatment usually required by conventional processes. The fine powders which are compacted using a cold isostatic press or a mechanical press are themselves reactants and undergo highly exothermic reactions once heated to the ignition temperature. High temperature synthesis occurs within intimate powder mixture, transforming the powders into compounds corresponding to the ratio of the reactants. The heat evolved during the reaction is the driving force that sustains and propagates the reaction throughout the body of the reactants [33, 36]. In the meantime, the high intensity of heat causes the powder compact to be heated to a high temperature just below the melting points of the compounds formed and thus cause rapid diffusion bonding of powder particles; leading to sintering of the powder.

In case of reaction sintering of TiAl, the reaction initiates at 660° C and is accompanied by the formation of the transient liquid [33] often contains a fraction of residual porosity arises from the green compact the sintered body pores due to kirkendall effect , porosity associated with gas evolution due to volatilization and molar volume defects due to intrinsic differences in the density of the reactants. Therefore pressure must be applied in some form during reactive sintering to synthesize and densify the product simultaneously].

1.6.2 Hot Pressing

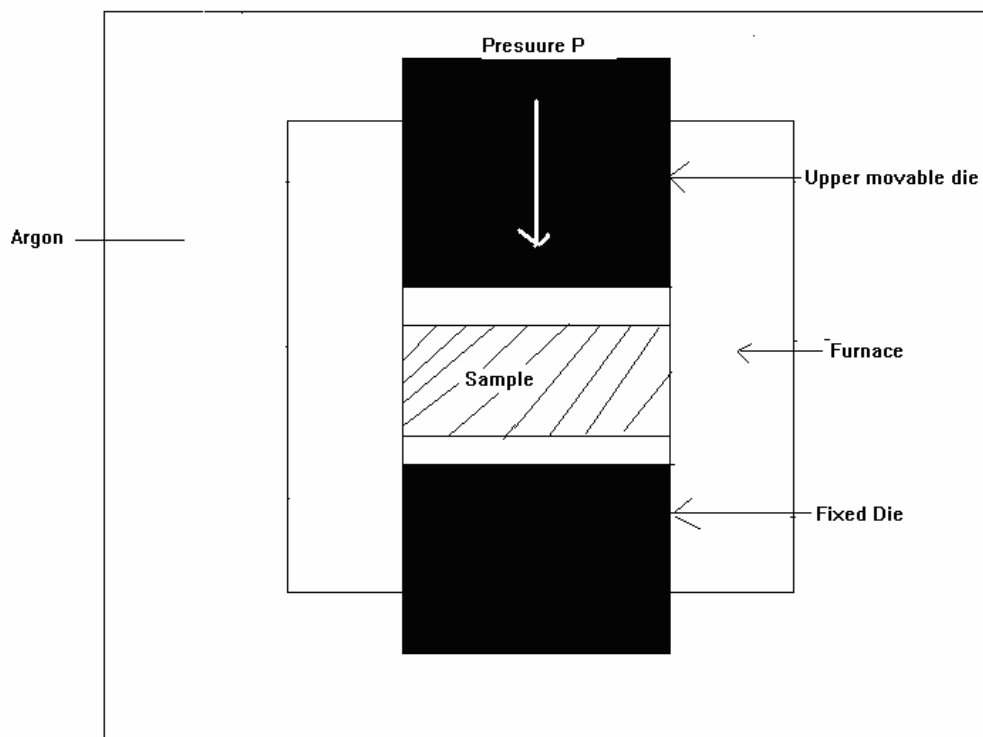


Figure1.9: Schematic diagram of hot pressing furnace used for consolidation powders

Hot pressing process is widely used to consolidate metal and ceramic powders to full density with controlled microstructure. In the process pressure and heat are applied to the green compact simultaneously as shown in the Figure 1.9 [33, 38]. Uniaxial pressure can be applied statically or dynamically. To prevent oxidation vacuum or controlled inert atmosphere such as argon is required.

Conventional titanium alloys like Ti -6Al- 7NB can be sintered under vacuum with temperature at 1250° C[38,39] but for the sintering of gamma based TiAl alloys for example γ - TAB higher temperature around 1350° C is to be chosen to obtain low porosity [39]. During the hot pressing the mold provides the component with desired shape. Heat can be provided directly (induction or wire resistance) or indirectly (convection or radiation). The main advantage of this process in comparison to the pressure less sintering is the reduction in the process time due to the application of the pressure [38]

1.6.3 Spark Plasma Sintering

Spark plasma sintering is new technique which uses direct current electrical field to heat the powder compact rapidly at high rate of 600° C / Minute, while a pressure is being applied to the powder compact. Hence the sintering process is generally very fast. The current passes through the graphite die as well as the powder compact in case of conductive samples. The heat is generated internally in contrast to the conventional hot pressing. Thus fully sintered components can be formed in very short period of time. When sintering TiAl alloys, CaO powder is generally used as a parting agent which prevents the chemical reaction between the graphite die and TiAl based alloy powder compact.[40] . Figure 1.10 shows a schematic diagram of the set up used for spark plasma sintering.

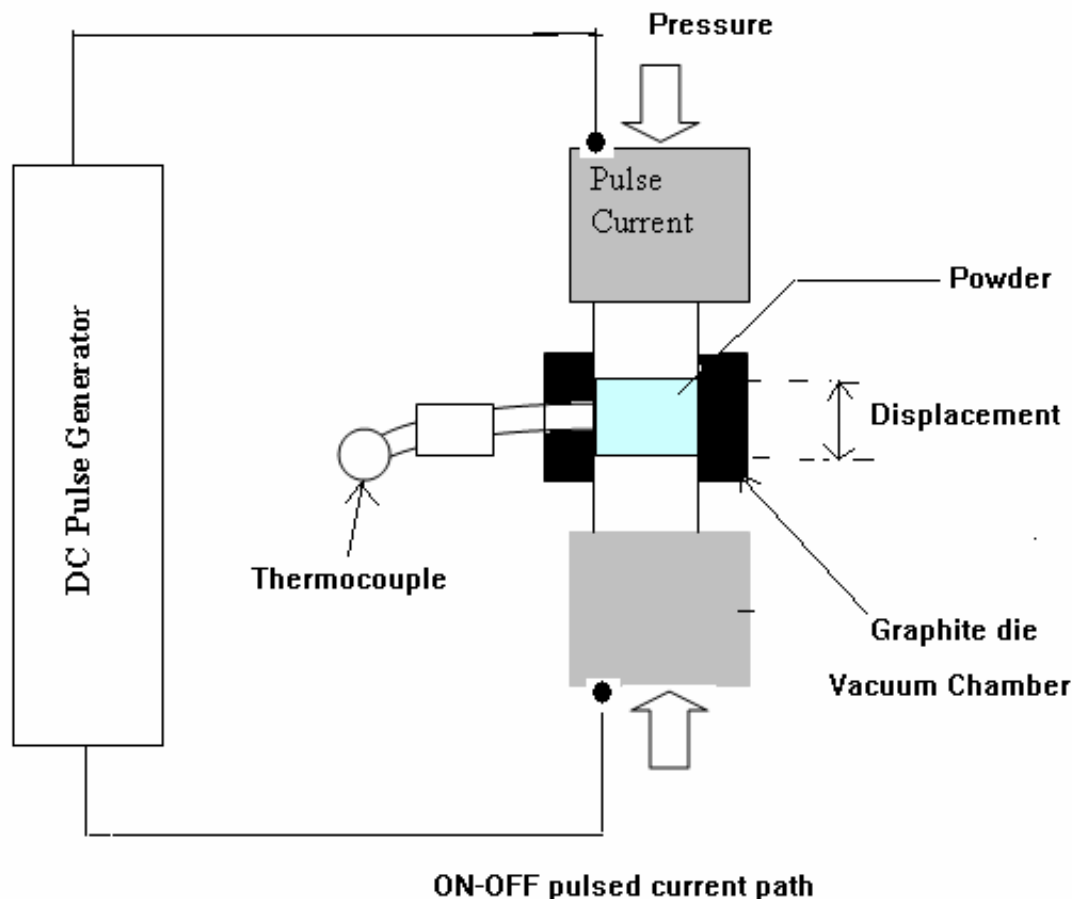


Figure 1.10: Schematic diagram of the set-up of spark plasma sintering [40]

1.6.5 Hot Isostatic Pressing

Hot isostatic pressing (HIPping) is well established technique for the consolidation of metal and ceramic powder metal castings are also often hot isostatically pressed to remove porosity formed during casting process [46]. Isostatic pressure is applied to a powder or compact sealed in a container at an elevated temperature to achieve significant powder compaction and inter-particle diffusion bonding which lead to formation of a sintered body. This process usually results in fully dense body although partially dense bodies can be produced intentionally [38,45]. The compact is canned, vacuumed and sealed.

For titanium alloys and TiAl based alloys canning can be done with titanium can [46], pyrex glass tube or stainless steel can [43,46]. During the process, the

Chapter 1: Introduction and Literature Review

compact is subjected to equal pressure from all sides as shown schematically in (Figure 1.11) . The pressurization medium in the furnace is normally inert gas.

Hipping pressure and Hipping temperature are critical process parameters that dictate the microstructure of the as-HIPped [[40, 42]. Higher hipping temperatures are not necessarily an advantage and can result in coarser microstructures [42] The fine and isotropic microstructure without requiring thermo-mechanical treatment can be achieved which are independent of the compact sizes [42]. Sub micrometer microstructure with the grain size of 180nm can be produced from mechanically alloyed amorphous powders by hot isostatic pressing [44]. For the particular compositions uniform duplex and fully lamellar microstructures can be achieved by optimising the Hipping process parameters [45].

In the previous research it has fine and homogeneous equiaxed microstructure with a grain size 2.0 μm out of Ti-47Al-4 (Nb, Mn, Cr, Si, B) (in at%)powder also called as γ -Tab has been achieved [42].The Hipping temperature used was 1025° C with the pressure of 200Mpa for two hours. Dense sheets of thickness 250-300 μm was produced via powder metallurgy route involving tape casting. The hipping temperature was 1100° C under pressure of 130MPa for 15 minutes. Although oxygen content of the sheet after hipping was found to be much higher, presumably introduced during decanning process but still but still fined grained near gamma microstructure with average grain size of 3 μm was obtained [43].

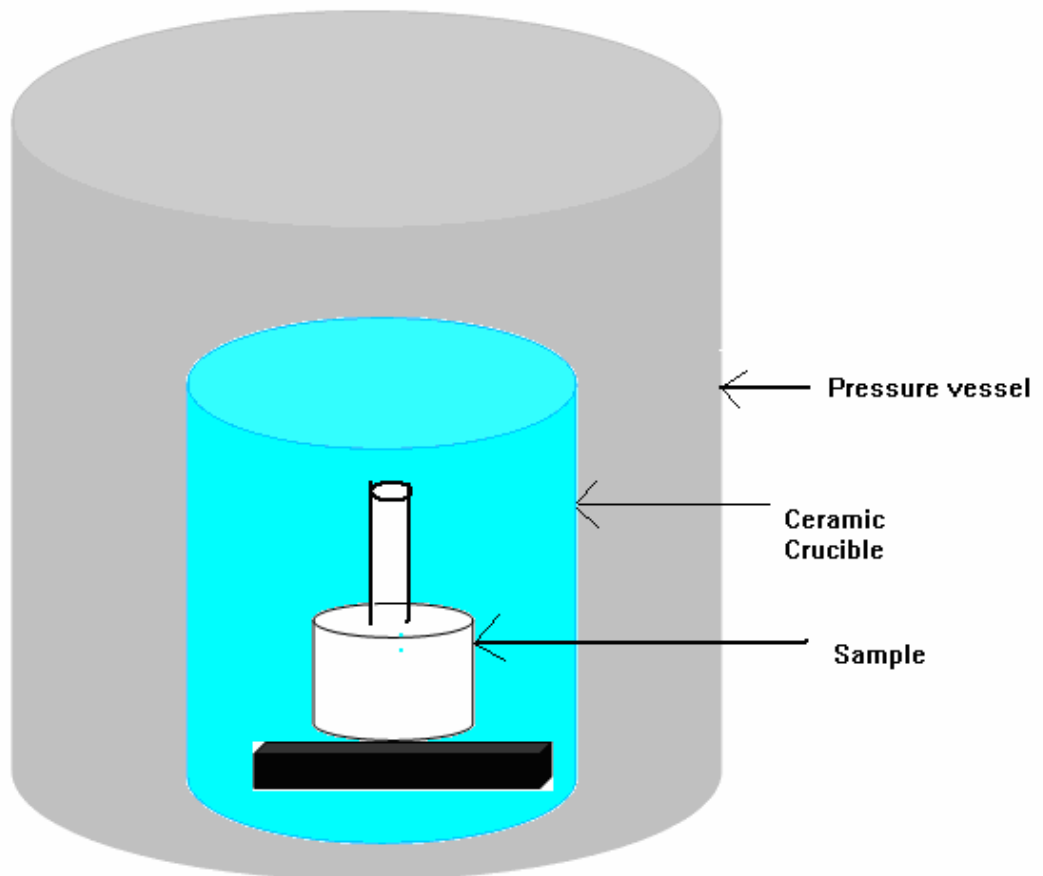


Figure 1.11: Schematic diagram of the set-up of a hot isostatic press vessel

Metal powder consolidation comprises an initial process of random packing and subsequent of powder compaction and pore closure. Each of these processes involves. Like in all material transport mechanism structural geometry, material properties and processing condition are the key on which active mechanisms and their rate depends. Accurate understanding of the important mechanisms, their interactions and their absolute and relative rate is required to predict consolidation behaviour [24][38].

1.6.4 Equal Channel Angular pressing/extrusion

Equal channel pressing or extrusion or pressing is bulk severe plastic deformation process that has effectively been used to produce ultra refine or nano structured bulk materials. The starting materials may either be bulk or powdered based compacts [54] . For TiAl ECAP often needs to be conducted at higher temperature at about 1000°C or greater. There is important benefit using ECAP/ECAE using elemental Ti and Al powders as it reduces the extrusion /consolidation pressure requirements compared to extrusion and consolidation of intermetallics phases [54,55].

1.4 Secondary processing

The sintered materials are often subjected to secondary processing to increase its density and improve the inter-particle bonding. The major process used for secondary processing of sintered bodies is forging. Forging is a process by which metal is heated and shaped by plastic deformation through applying compressive force. The compressive force can be applied by a power hammer or press. The main objective is to refine the grain and improve the physical properties of the material. Xu and Lin successfully carried out the forging of the canned as - cast TiAl alloy which has a high level of porosity, detrimental β phase and a nearly full lamellar microstructure and were able to get the fine homogeneous microstructure with superior tensile properties . [53] For the gamma alloys containing more than 47 at. % of aluminium content grain refinement is the most common method of decreasing the temperature at which superplasticity is observed. Previous research shows that through the multi step forging of cast and hiped Ti48Al- 2Crin at.%, fine equiaxed grain structure with mean size of $0.3\mu\text{m}$ was produced. Superplasticity of 355% at 800°C was obtained [54]. A billet made from Ti- 47Al-4(Nb, Mn, Cr, Si, B) powder by hot isostatic pressing was successfully forged at 850°C and the material showed superelastic parameters which were attractive for technical application Grain size obtained after hipping which was $2.0\ \mu\text{m}$ was refined to $0.9\ \mu\text{m}$ while microstructure still remained homogenous equiaxed. Tensile specimen cut from the forged material showed superelastic properties at 910°C and 1000°C with reasonable strength of 130MPa and 50MPa at the respective temperatures [42].

Chapter 1: Introduction and Literature Review

So far Cast and wrought TiAl materials have been employed to manufacture the simple and small components like turbo charger turbine wheels and automotive engine valves. Precision casting methods are often associated with poor fluidity, easy cracking at stress concentration portion as well as difficulty in repair, whereas wrought materials can be used for rolling thin plates and automotive engine valves as well. But for the fabrication of large TiAl components having complex shapes and high dimensional precision suitable process needed to be developed to expand the application of TiAl based alloys [53, 56].

.A new Ti-42Al-5Mn(at%) alloy which featuring capabilities was developed after successfully hot forging after heating 1300° C and subsequent heat treatment at 1200° C for two hours.[52]. Prototype complex shaped as shown in Figure 1.12 components were fabricated out the newly developed TiAl alloy [56].

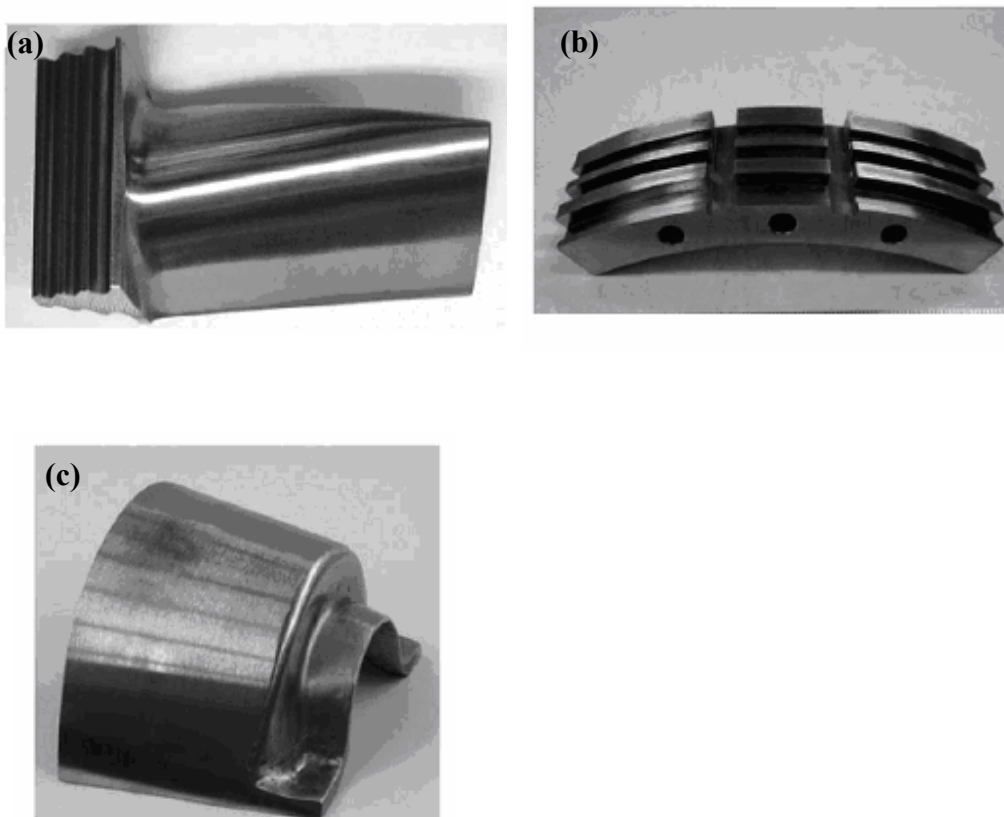


Figure 1.12: Examples of TiAl based prototype components produced by forging : (a) Turbine blade (b) shroud part of the turbine and (c) half of top cone of turbine [56]

References

1. A. Lasalmonie “Intermetallics why is it so difficult to introduce them in gas turbines”, intermetallics Vol 14, 10-11, (2006), p. 1123
2. G. Wegmann, R. Gerling, F.-P. Shimansky “Temperature induced porosity in hot isostatically pressed titanium aluminide alloy powders” Vol 14, 10-11, (2006), p. 1123
3. F. Appel, U.Brossman, U.Christoph , S.Eggert , P.Janshek , U.Lorenz , et al. Advanced materials. Wiley-VCH Weinheim, Vol 2,(2000) (11) p. 699-720
4. C. Leyens and P. Manfred “Titanium and Titanium Alloys” Weinheim-VCH (2003)
5. D.P Delo., H, Piehler “Early stage consolidation mechanisms during hot isostatic pressing of Ti-6Al-4V powder compacts” Acta. Materiala. Vol 47, (1999) p. 2841-2852
6. Y.W.kim and D. M Dimiduk “ Progress in the understanding of gamma titanium aluminides “ Journal of Materials,1991,43 (8), 40-47
7. F.H. Froes, C. Suryanarayana, C. M. Ward-close “Synthesis/processing of light weight metallic materials” the minerals.Metals and the Materials society ,TMS annual meeting1995
8. S. Djanarthany, J. -C. Viala and J. Bouix “ An overview on monolithic titanium aluminides based on Ti_3Al and $TiAl$ ” Materials Chemistry and Physics, Vol. 72, 3, (2001), p.301
9. Y. Mishin and Herzig “ Diffusion in the Ti-Al System”, Acta materiala. 48(2000) 589-623
- 10.R.K. Gupta, M. Arumugam, M.K. Karthikeyan, Bhanu Pant and B.R. Ghosh “Investigation of ultrasonic indications in Ti alloy (Ti6Al4V) hot formed hemisphere Engineering Failure Analysis”, Vol 14, 7, (2007), p.1286
- 11.R.R. Boyer “An overview on the use of titanium in the aerospace industry” Materials Science and Engineering A, Vol 213, 1-2, (1996), p. 103
12. X. Wu “Review of of alloys and process development of TiAl Alloys “, Intermetallics 14 (2006) 1114 – 1122

Chapter 1: Introduction and Literature Review

13. T. Tetsui, K. Shindo ,S. Kaji, S. Kobayashi and Masao Takeyama “Fabrication of TiAl components by hot forging and machining”, *Intermetallics*, Vol. 13, 9, (2005), p. 971
14. T. Novoselova, S. Celotto, R. Morgan, P. Fox and W. O'Neill “Formation of TiAl intermetallics by heat treatment of cold-sprayed precursor deposits *Journal of Alloys and Compounds*”, Vol. 436, 1-2, (2007), p. 69
15. Dr. K Xia 430-460 unit 1: Advanced metallic materials
16. M.Yamaguchi, H.Inui and K. Ito “High temperature structural intermetallics ”, *Acta materiala* 48 (2000) 307-322
17. Y.Mishing and Chr. Herzog “Diffusion in the Ti-Al system” *Acta materiala* 48 (2000) 589 623
18. M.Thomas, J.L. Raviart, F.Popoff “Cast and PM processing development in Gamma alloys” *Intermetallics* 13 (2005) p.944-951
19. G. Cao, L. Fu, J. Lin, Y. Zhang and C. Chen “The relationship of microstructure and properties of a fully lamellar TiAl alloy” *intermetallics*, Vol. 8, 5-6,(2000) p. 647
20. Y.-W kim “Strength and ductility in TiAl alloys intermetallics” Vol. 6, 7-8 (1998),p.623
21. C.T. Liu and P.J. Mazia “Microstructural control and properties of dual-phase TiAl intermetallics”, Vol 6, 7-8 1998 p (623-628)
22. O. H.Mall J.Mc tiernam “PM TiAl alloys: The sky’s the limit “ *Metal powder report*, Vol. 55,(2000) p. 18
23. K. Maruyama, R Yamamoto , H. Nakakuki, N. Fujitsone “Effects of Lamellar spacing , volume fraction and grain size on creep strength of fully lamellar TiAl alloys” *Materials science and engineering A*, Vol. 239 (1997) p.419 428
24. Y.mutah, S.J. Zhu, T. Hansen, S.kurai, Y. Mizuhara “Effects of fatigue growth in TiAl intermetallics at elevated temperature” , *materials science and engineering A*323 (2002) 62-69
25. Dr. Deliang Zhang University of Waikato, “Notes for paper ENP-512” (2006)
26. D.Hue , “Effects of boron addition tensile ductility in lamellar TiAl alloys” , *Intermetallics* ,Vol. 10, 9,(2002) p. 851-858

Chapter 1: Introduction and Literature Review

- 27.R, Gnanamoorthy, Y.Mutoh, Y. Mizuhara “Effects of Niobium addition on the sustained load cracking characteristics in lamellar microstrcture gamma base TiAl “ Materials science and Engineering A , Vol. 203, 1-2,(1995),p. 348
- 28.S.kim, G.D.W.Smith, S.G .Roberts, A.Carezo “Alloying elements characterization in gamma based titanium aluminides by APPFM “Material Science and Engineering A 250 (1998) 7782
- 29.H. Qiang Ye “Recent developments in Ti_3Al and TiAl intermetallics research in china” Materials Science and Engineering A, Vol. 263, 2, (1999), p. 289
- 30.J. Mathew Jr Donachie, Titanium A Technical guide, Park OH ASM international ,2000
- 31.J. Stevan , Gerdamann , Titanium process technologies , Albany , Oregon
32. R. Gerling , H.Clemens and F.P. Scimensky, “Powder metallurgical process of intermetallic gamma titanium aluminides” Advanced materials 2004,6,No1-2
- 33.C.Z. Han, “Consolidation of Al-TiO₂ and $Ti_3Al - Al_2O_3$ ”, Phd Thesis ,University of Waikato
34. F. Wenbin,H .Lianxi, H. Wenxiong, W. Erde,L. Xiaoqing, “Microstructure and properties of TiAl alloy prepared by mechanical milling and subsequent reactive sintering” Materaials science and engineering: A,Vol. 403 (2) (2005) p.186
- 35.T. Novoselova, S. Celotto, R. Morgan, P. Fox and W. O'Neill “Formation of TiAl intermetallics by heat treatment of cold-sprayed precursor deposits” Journal of Alloys and Compounds, Vol. 436, 1-2, (2007), p. 69
- 36.L.M. Peng, Z. Li, H. Li, J.H. Wang and M. Gong “Microstructural Characterization and Mechanical Properties of TiAl–Al₂Ti₄C₂–Al₂O₃–TiC in situ composites by hot-press-aided reaction synthesis”, Journal of Alloys and Compounds, Vol. 414, 1-2, (2006), p. 100
- 37.E. David, Alman , “Reactive sintering of TiAl–Ti₅Si₃ in situ composites” Intermetallics, Vol. 13, 6, (2005), p. 572
- 38.V. Viswanathan, T. Laha, K. Balani, A. Agarwal and S. Seal “Challenges and advances in nanocomposite processing techniques” Materials Science and Engineering: R: Reports, Vol 54, 5-6, 30 (2006), P 121-285

Chapter 1: Introduction and Literature Review

39. R. Gerling, E. Aust, W. Limberg, M. Pfuff and F.P. Schimansky “ Metal injection moulding of gamma titanium aluminide alloy powder Materials” Science and Engineering: A, Vol. 423, 1-2, (2006), p. 262
40. K. Matsugi, N. Ishibashi, T. Hatayama and O. Yanagisawa “Microstructure of sparksintered titanium-aluminide compacts” Intermetallics, Vol.4,(1996), p. 457-467
41. Ulrike Habel and Brian J. McTiernan HIP temperature and properties of a gas-atomized γ -titanium aluminide alloy Intermetallics, Vol.12, 1, (2004), p. 63
42. G. Wegmann, R. Gerling, F-P Schimansky, H. Clemens and A. Bartels “ High-temperature mechanical properties of hot isostatically pressed and forged gamma titanium aluminide alloy powder” , Intermetallics, Vol. , 5,(2002), p. 511
43. A.G. Adams, M.N. Rahaman and R.E. Dutton “Microstructure of dense thin sheets of γ -TiAl fabricated by hot isostatic pressing of tape-cast monotapes “Materials Science and Engineering A In Press, Corrected Proof
44. M. R. Shagiev, O. N. Senkov, G. A. Salishchev and F. H. Froes” High temperature mechanical properties of a submicrocrystalline Ti–47Al–3Cr alloy produced by mechanical alloying and hot isostatic pressing” Journal of Alloys and Compounds, Volume 313, Issues 1-2, 15 December 2000, Pages201-208
45. L. Zhao, J. Beddoes, D. Morphy and W. Wallace “Microstructure and mechanical properties of a PM TiAl-W alloy processed by hot isostatic pressing “Materials Science and Engineering A, Vol. 192-193, 2, 28 February 1995, p. 957
46. M.Usta, H.Wolfe, D.J. Denquette,N.S. Stoloff, R.N. Wright “Thermo-mechanical grain refine ment in gamma(γ) bound TiAl intermetallics”. Material Science and Engineering A 359(2003) 168
47. Y.Wu, S.K.Hwang , “Microstructural refinement and improvement of mechanical properties and oxidation resistance in EPM TiAl based intermetallics with Yttrium addition”, Acta materiala 50 (2002) 1479-1493

Chapter 1: Introduction and Literature Review

- 48.Q.U.Shengguan, Li Xiaoqiang, Li Yuanyuan, Hu Lianxi and Wang Erde “Manufacturing a TiAl alloy by high energy ball milling and subsequent reactive sintering “ Rare metals Vol 25, (2006), p.21
- 49.W.H Tian and Nemoto “Effect of carbon addition on the microstructures and mechanical properties of gamma- TiAl alloys” ,*Intermetalics* Vol.(5) (3) (1997) p.237
- 50.M.Lamirand,J.I.Bonnentian,G.Ferriere,S.Guerin J.P. Chevalier “Relative effects of chromium and niobium on microstructure and properties as a function of oxygen content in TiAl alloys” *Scripta materialia* vol(56) ,(5) ,(2007), p.325
- 51.F.Appel, R.Wagnner “Microstructure and deformation of two phase γ titanium aluminide “ *Material science and engineering R*(22) (1998) 187-268
- 52.A Paul, Barlolotta and L David, Krause Glenne research center Cleveland Ohio Titanium aluminide “Application and in the high speed civil transport NASA/TM 1999-209071”
- 53.X.J. Xu, J.P. Lin, Y.L. Wang, J.F. Gao, Z. Lin and G.L. Chen “Effect of forging on microstructure and tensile properties of Ti-45Al-(8-9)Nb-(W,B,Y) alloy” *Journal of Alloys and Compounds*, Vol. 414, 1-2, (2006), p. 175
- 54.K Morsi and S.Goyal “Equal Channel angular pressing followed by Combustion Synthesis of Titanium Aluminides “ *Journal of Alloys and Compounds* Vol. 429, 1-2 (2007) p. 21
- 55.M.A. Munoz- Morris, L.Gutierrez-Urrutia and D.G. Morris Effect of “Equal channel angular pressing on strength and ductility of Al-TiAl composites” *Materials Science and Engineering A* Vol. 396, 1-2 (2005) p.3
- 56.Toshimitsu Tetsui,Kentaro Shindo,Satoshi Kaji,Satoru Kobayashi and Masao Takeyama “Fabrication of TiAl components by hot forging and machining” *Intermetallics*, Vol. 13, 9, (2005), p. 971

CHAPTER TWO :

Experimental Procedure

Chapter Two: Experimental Procedure

This chapter describes the experimental procedure used in the course of research undertaken in this ME research project. This comprises of the materials used, processes involved, sample preparations, techniques and facilities employed for analysing the samples.

2.1 Powder Compaction

Pre-alloyed powders with the three different compositions TiAl-1.0X, TiAl-1.5X and TiAl-2X supplied by Titanox Development Ltd were used for the experiments. The three powders were called TAX1, TAX2 and TAX3 powders respectively. The powders were first pressed mechanically using rigid die and a hydraulic press and then by Cold Isostatic Pressing (CIP) prior to hot isostatic pressing .The powder compact formed after cold isostatic pressing was dense and its density distribution was more homogeneous.

For producing each powder compact 100 g of powder was poured into a HB tool die with a cylindrical cavity of 40mm of diameter. The powder in the die was then pressed using a hydraulic press. A pressure of about 35MPa was applied and was held for 10 minutes. This pressure was enough to hold the powder together. Then the compact was transferred to a cold isostatic press as shown in Figure 2.1.



Figure 2.1 Cold Isostatic press used in compacting the powder

For the preparation of samples for cold isostatic pressing, the die pressed pellets were placed in rubber gloves. The gloves were evacuated and sealed. The isostatic press design was of the screw thread closure type with the internal chamber

Chapter Two: Experimental Procedure

dimensions of $\Phi 72\text{mm} \times 300\text{mm}$ deep. The samples were placed in a wire cage and the cage was suspended in the chamber. The pressurisation fluid used was acetylene glycol along with corrosion inhibitor additives. The pressure used was 200MPa which is the maximum capacity of the press and was held for 5 minutes, which was sufficient for cold isostatic pressing. After cold isostatic pressing, the dimensions of the cylindrical compact were measured as $\Phi 35\text{mm} \times 40\text{mm}$. The green density of the compact was measured to be between 60 to 65% of the theoretical density of the TiAl was taken as 3.9 g/cm^3 .

2.2 Degassing and Canning of the powder Compacts

The pellets obtained after cold isostatic pressing were placed in a cylindrical 316 stainless steel can (316SS) with the clearance of about 0.5mm between the pellet and the can. Then a 316SS tube with 1mm internal diameter and a thickness of 0.6 mm was welded on to lid of the 316SS steel can. The lid was welded on the top of the can as shown in Figure 2.2 Tungsten inert gas (TIG) welding was used for the whole welding. The can was then evacuated before it was sealed.



Figure 2.2: Canned sample before de-gassing and sealing

Chapter Two: Experimental Procedure

For de-gassing hollow tube was connected to a vacuum pump to be evacuated to a vacuum level of -100KPa while the can was being held at temperature of 325° C for 1 hour. Then the tube press-sealed using a hydraulic press and specially designed fixture as shown in Figure 2.3.



Figure2.3: The Pressing die and the fixture used for press-sealing the tube

After press-sealing the tube of the can, the screws of the fixture was tighten up and the can was allowed to cool to room temperature. After this the tube was cut using a hack-saw and the end of the tube was sealed by TIG welding as shown in Figure 2.4



Figure 2.4: Sealed cans after de-gassing and press - sealing and welding

2.3 Powder Consolidation by Hot Isostatic Pressing

The hot isostatic press that was used for consolidating the powder compacts were of the model CPSI SL-1 and is located in the large scale laboratory at the University of Waikato as shown in Figure 2.5. The press is designed for simultaneous heating and isostatically pressing powder compacts sealed in containers. The furnace has dimensions of $\Phi 12.5\text{cm} \times 25\text{cm}$ and is capable of operating at temperatures ranging 25 to 1400°C and at pressures in the range of 0.1 to 207MPa.

The pressure vessel



Compressor



Figure 2.5 : Hot Isostatic Press

The pressurisation medium used in the HIP is argon. Heating was done at the rate of $10^{\circ}\text{C}/\text{minute}$ and it took about two hours to reach 1200°C . Then the furnace was held at 1200°C for two hrs with pressure of 200MPa ,followed by furnace cooling till the temperature went down to 150°C and air cooling there after. Figure 2.6 shows the temperature – time and pressure – time graphs that reflect the process condition used in the HIPping experiments.

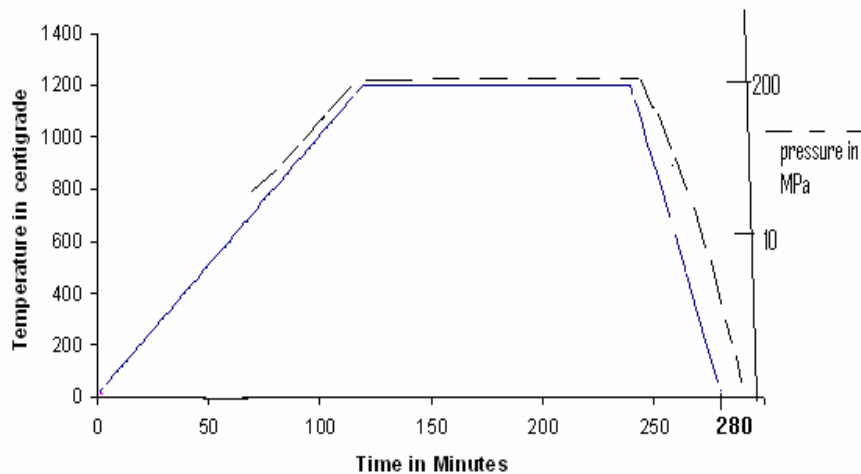


Figure 2.6: Graphical representation of temperature and pressure change during the HIPping process

2.4 Secondary Processing of the Consolidated Sample

After the consolidated sample made using Tax2 powder was taken out of the stainless steel can, it was sectioned into two equal halves along transverse direction. Then one of the two halves was placed in a stainless steel can and the space between the sample and the can was filled with aluminium oxide powder as release agent. The top of the can was covered with a stainless steel lid and sealed using TIG welding as shown in Figure 2.7(a). Open die forging along the longitudinal direction was performed. The two halves of an open die were preheated to 200°C, and the canned samples was heated 1160° C before forging.



Figure 2.7: (a) Hipped Tax2 concealed by stainless steel can before Forging
(b) Side view of the disk produced by forging of the consolidated sample and (c) Planar view of the disk which a tensile test specimen being cut from the disk

2.5 Tensile Specimen Preparation

Tensile testing specimens rectangular in shape with a gauge length of 12 mm, and a rectangular cross-sectioned shape of 4mm in width and 3mm in thickness (Figure 2.8) were cut using Electrical discharge machining (EDM)wire cutter. The machine uses copper wire as a spark eroder and water as a coolant.

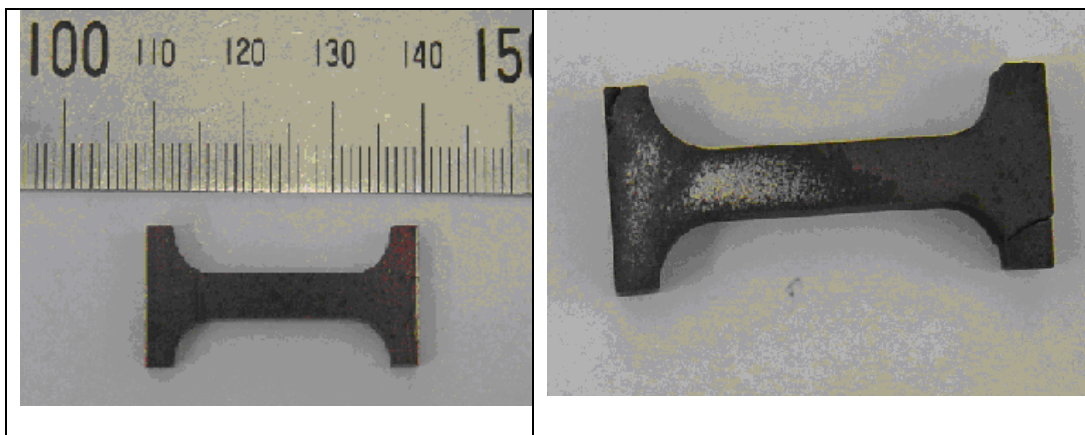


Figure 2.8 (a) Tensile specimen from Hipped sample
(b) tensile specimen from forged sample

2.6 Mechanical Testing

Tensile properties (strength and elongation to fracture) of the specimens of all the three compositions were measured at different temperatures using a Instron 4042 tensile testing machine with a 5KN load cell. The strain rate used for room temperature testing was $6 \times 10^{-5} \text{ s}^{-1}$ at room temperature while strain rate used for 800°C and 900°C was of $1 \times 10^{-4} \text{ s}^{-1}$. High temperature tensile testing was conducted under flowing argon protection.

2.7 X-Ray Diffractometry

X-Ray diffraction (XRD) was used to study the crystallographic structure and phases of the as received pre-alloyed powders and sintered and forged samples. The XRD equipment used was Philips X-Ray Diffractometer using Cu- K α

Chapter Two: Experimental Procedure

radiation (wavelength $\lambda=1.54 \text{ \AA}$) . The X-ray tube was set at 40kV and 40mA. Scan range with a value of 2Θ from 12 to 90° with scan step of $.05^\circ$ were used. The results were interpreted using JCPDF database software.

2.8 Density Measurement

Bulk density and the relative density of consolidated samples were measured using Archimedes principle using water as immersing liquid. Equations 2-1 and 2-2 were used to calculate the measured density and relative density of the samples respectively

The formula used was:

$$\text{Density Measured (} D_m) = \frac{\text{Weight of the sample in air}}{\text{Difference of weight in air and water}} \quad \text{----- (2-1)}$$

$$\text{Relative Density (} D_E) = \text{Density Measured (} D_m)/\text{theoretical density of TiAl} \quad \text{----- (2-2)}$$

The theoretical density of TiAl was taken as 3.9 gms/cm^3

2.9 Microscopy and Particle Size Analysis

The consolidated samples and the powder samples were mounted in cold epoxy resin. Then the mounted samples were first ground using a series of emery papers (320, 500, 1000, 2000 and 4000). Then the final polishing was done using alumina particle suspension to obtain scratch free polished samples. Surface topography and microstructure of the samples were investigated using optical microscopy (Olympus BX60M) and scanning electron microscopy (SEM). The equipment used was Hitachi 4000 SEM equipped with energy dispersive spectroscopy (EDS).

Chapter Two: Experimental Procedure

Shimadzu SALD -2001 laser particle size analysis was used to determine powder particle size distribution. Powders were dispersed ultrasonically in distilled water for analysis

2.10 Microhardness Testing

Microhardness testing of the powdered samples of all the three compositions and that of consolidated samples were performed. The microhardness was measured using a LECO LM 700 Vickers microhardness tester .A Load of 25g and loading duration of 20 seconds was used for the consolidated bulk sample, whereas 10 g. of load for 20load duration seconds were used for testing the microhardness of the powder particles . 10 indents for the powdered samples and 10 indents for each phase of the hipped and forged samples were produced for one average measurement.

CHAPTER THREE:

Results and Discussions

3.1 Powder Characterization

Figure 3.1 shows the images of the cross sections of the particles in the three as - received powders. The shape of the powder particle is irregular and generally equiaxed. The particle sizes range from. The particle size varies from $2\mu\text{m}$ to $25\mu\text{m}$ for Tax1 powder, $1\mu\text{m}$ to $5\mu\text{m}$ for Tax2 powder and from $0.5\mu\text{m}$ to $20\mu\text{m}$ for Tax3. There are some agglomerates present. There is no contrast within the particle suggesting that the powder particle consists of only single phase. Figure 3.2 shows the powders particle size distribution curves of the three as received Titanox powders. These particle size distributions were determined using laser particle size analysis as mentioned in Chapter 2. For Tax1 powder the particle size ranges from $1\mu\text{m}$ to $300\mu\text{m}$ with mean diameter of $28.33\mu\text{m}$. Tax2 powder shows the particle size ranging from $0.8\mu\text{m}$ to $120\mu\text{m}$ with mean diameter of $30\mu\text{m}$, whereas Tax3 powder has smallest particle mean diameter of $9\mu\text{m}$ with particle size ranging from 0.78 to $36\mu\text{m}$. The particle size of the powders determined from the powder particles analysis are considerably larger than those determined by the SEM examination of the cross section of the powder particles. The discrepancy is likely to be due to the agglomeration of the small particles which was not effectively eliminated during particle size analysis.

The powders were chemically analysed using the LECO combustion technique to determine that the oxygen content .It was found that oxygen content of the Tax1 Tax2 and Tax3 was 1.7wt%, 2.5wt% and 3.1wt%, respectively which is remarkably high. The average microhardness of the powder particles measured using 10 g load and 20 seconds loading duration was 412 ± 23 , 350 ± 30 , and 406 ± 10 in Vickers hardness (VHN) respectively for Tax1, Tax2 and Tax3 powders.

XRD patterns of the Titanox powders are shown in Figure 3.3. The predominate phase in all three powders is face centred tetragonal (f.c.t). TiAl phase as shown by the well defined XRD peaks. There is a small amount of minor phase which is likely to be Ti_3Al . Figures 3.4- 3.6 show high magnification images of cross section of powder particles and correspondingly EDS spectra. All EDS spectra show primary peaks of titanium and a aluminium. This explains the presence of TiAl and some titanium rich Ti_3Al peaks in the XRD patterns as discussed before. The other peak of

Chapter 3: Results and Discussions

the spectra is Pt peak from the Pt coating on the SEM samples. Composition analysis of the well defined. Majority of the peaks are of TiAl.

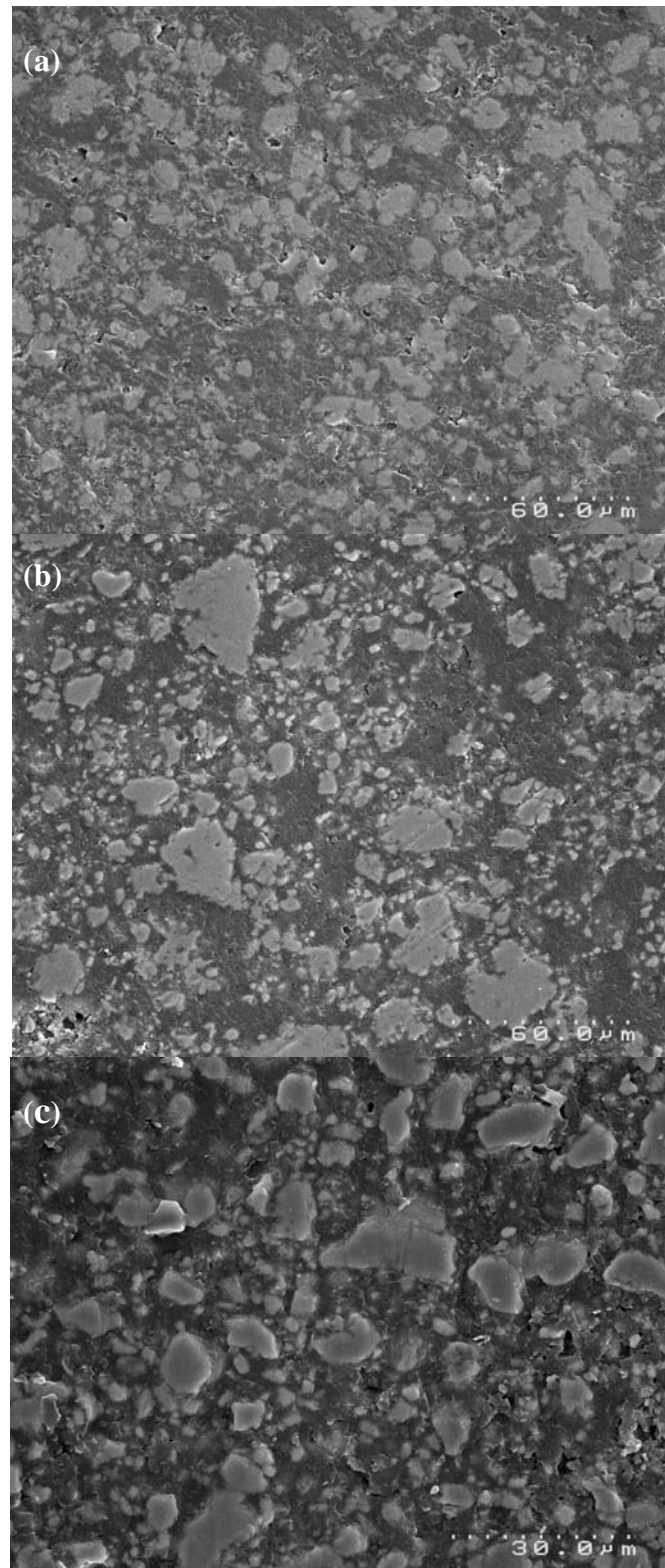


Figure 3.1: Powder particle morphology and size of the as received Titanox powders
(a) Tax1 powder, (b) Tax2 powder (c) Tax3 powder

Chapter 3: Results and Discussions

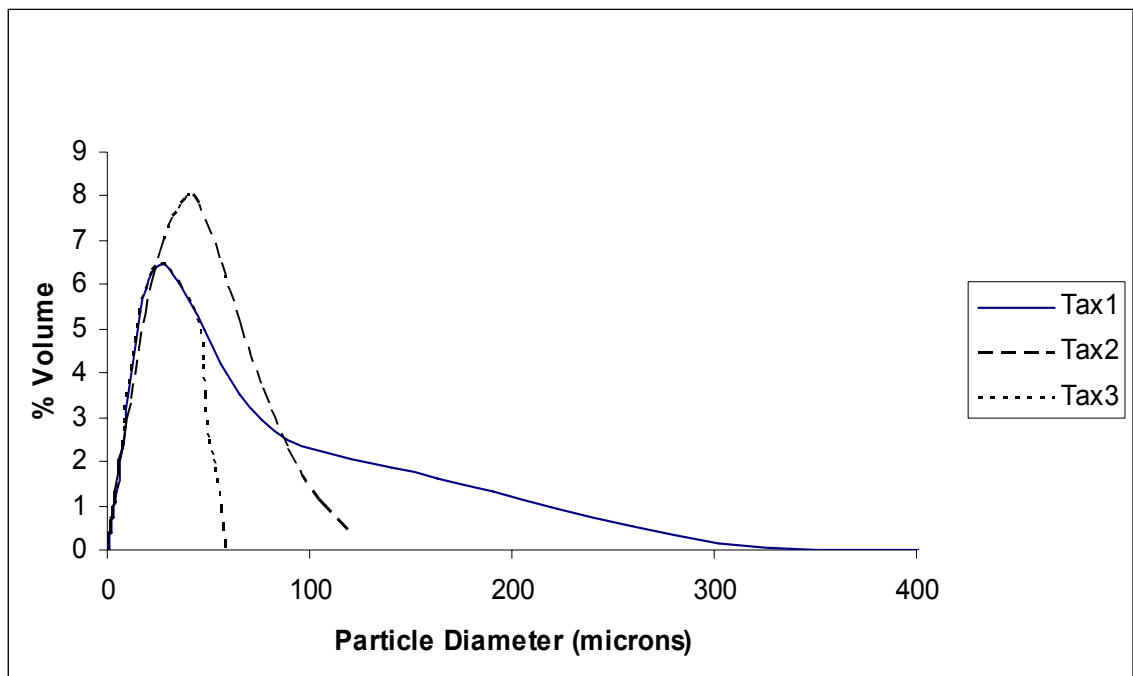


Figure 3.2 Normalised powder particle size distributions for the powders

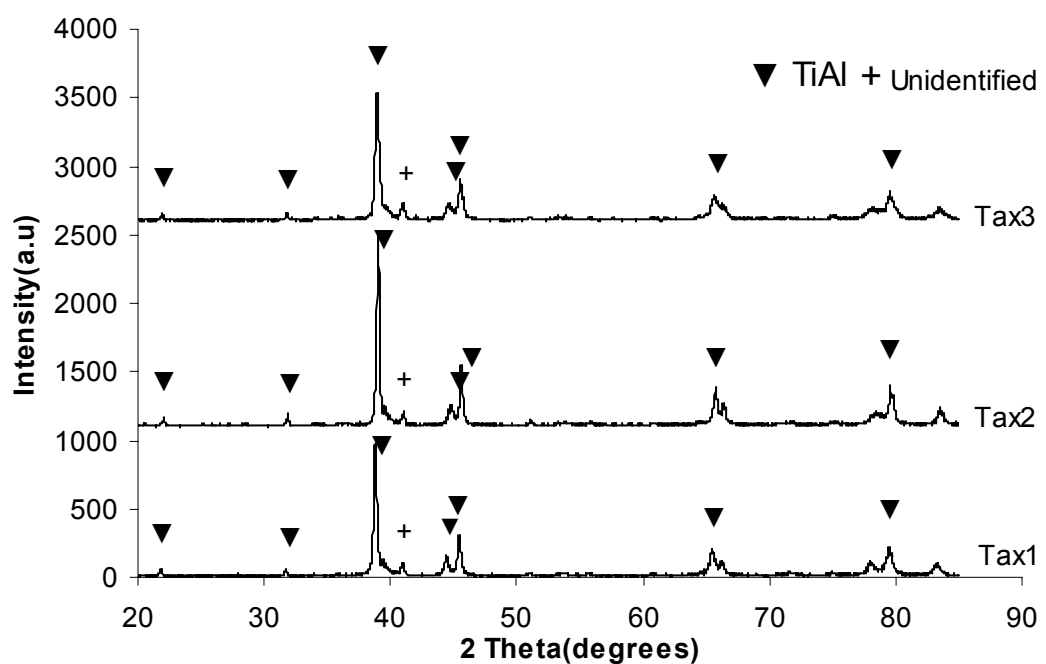


Figure 3.3 XRD Patterns and analysis of the as-received Titanox Powders

Chapter 3: Results and Discussions

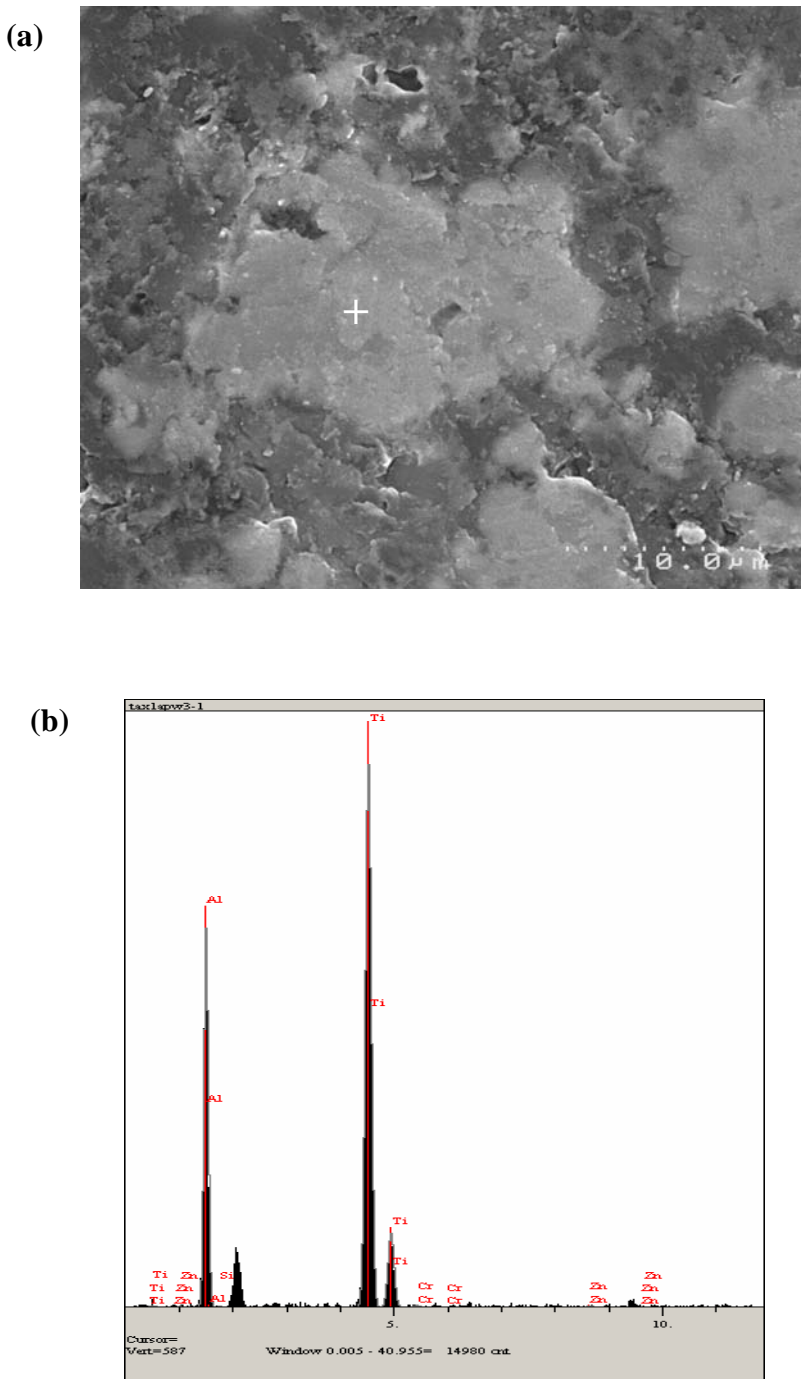


Figure 3.4: (a) Cross section of the particles in the Tax1 powder (b) EDS spectrum from the point shown by the cross in (a)

Chapter 3: Results and Discussions

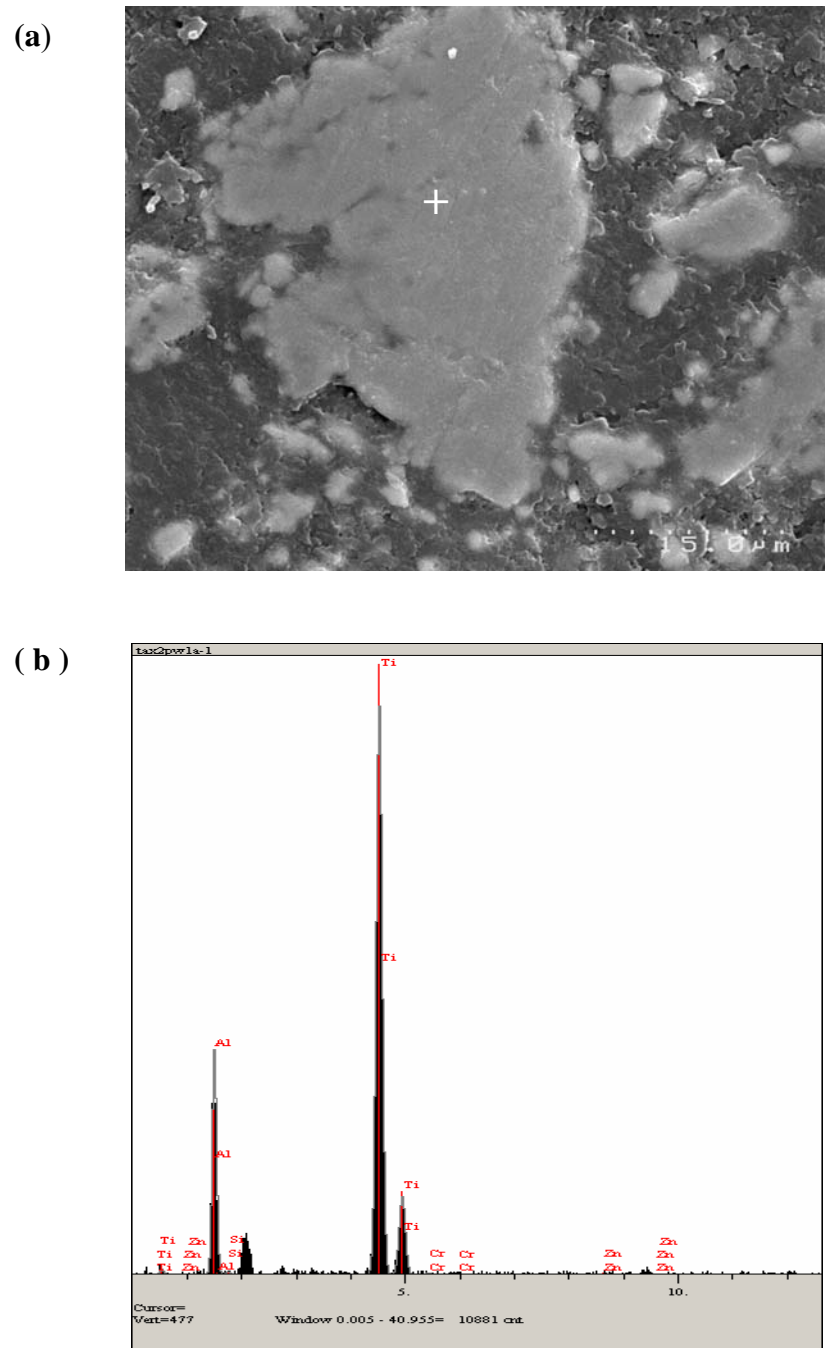


Figure 3.5 (a) Cross section of the particles in the Tax2 powder (b) EDS spectrum from the point shown by cross in (a)

Chapter 3: Results and Discussions

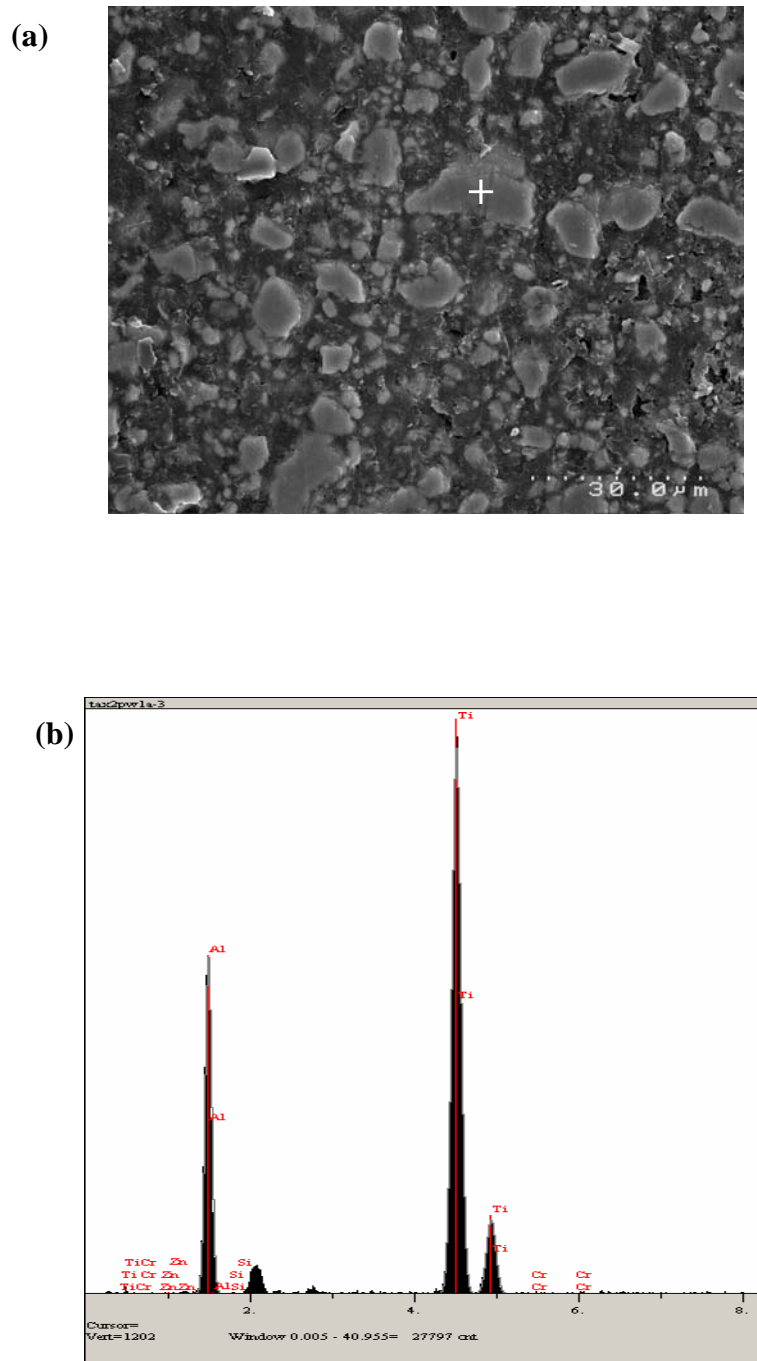


Figure 3.6: (a) Cross section of the particles in the Tax3 powder (b) EDS spectrum from the point shown by cross in (a)

Chapter 3: Results and Discussions

Table 3.1: Content (in at%) of different elements in the threes particles shown in Figure3.4-3.6 determined using semi-quantitative EDS analysis

Powders	Ti	Al	O	Si	Cr
Tax1	50.5	42.8	5.9	0.1	0.2
Tax2	47.9	24.5	26.8	.24	.3
Tax3	58.5	39.7	1.4	0.3	.1

. Point analysis has been done at the centre of the powder particle. For all the three powders compositions the peak with highest intensity is titanium peak .Second most intense peak is aluminium peak which is less intense for Tax2 powder of titanium and almost has same intensities for all the three compositions. Second major peak aluminium is slightly less intense for Tax2 than that for Tax1 and Tax3 powders as shown in Figure 3.4(b), 3.5(b) and 3.6(b).

Table 3.1 shows the concentration of different elements in atomic percent in the three powder particles shown in Figure 3.4-3.6 determined using semi-quantitative EDS analysis. The particle in the Figure 3.4 has 50.5at% titanium and 42.8at% of aluminium composition. The oxygen content was shown to be 5.9at%.There is small amount of silicon 0.1at% and chromium 0.2at% which may come from the raw materials used in for making the powders. For the powder particle in the Figure 3.5 the content of titanium is 47.9at% and that of aluminium is 24.5at% of the particle. Considerably high oxygen content of 26at% is shown by composition analysis of the particle and which is absurd and presumably may be because of some error on the part of the composition analysis and it is not in agreement with the results of bulk chemical analysis of the Tax2 powders which shows oxygen content to be 2.5wt% .The composition analysis of the particle shown in Figure 3.6 shows that titanium and aluminium content was 58.4at% and 39.7at% respectively and the oxygen content was 1.4at%.

3.2 Consolidation Behaviour of the Titanox Powders in Hot Isostatic Pressing

The relative density of the green compacts of all the three different compositions after uniaxial pressing under the pressure of 35MPa and cold isostatic pressing under pressure of 200Mpa were measured by measuring their weights and dimensions. The theoretical density of the TiAl was taken as 3.9g/cm³. It was found that the relative density of the green powder compact for was 67% for Tax1 powder, 69% for Tax2 and 64% for Tax3 powder.

The consolidated samples produced by hot isostatic pressing of the canned powder compacts at 1200°C for two hours under pressure of 200MPa for the three powders compositions are shown in the Figure 3.7 As shown in the Figure 3.7(a) the canned compact of Tax1 powder shranked by 9%in diameter and 7%in height after HIPping. The stainless steel can can be easily chipped from the material after HIPping suggesting that there was no reaction between the can and the powder compact. Relative densities of the consolidated samples were measured using Archimedes principle .The Relative density of the Tax1 was found to be 96%. The distributions of the pores in the HIPped sample were generally homogenous and sizes of the pores were in the range 1-3μm Figure 3.8(a). Also the distribution of the light grey phase with the size ranging from 0.5μm to 12μm in the major white phase is homogenous and equiaxed the concentration of the dark and grey phases are along the boundaries of the white phase.

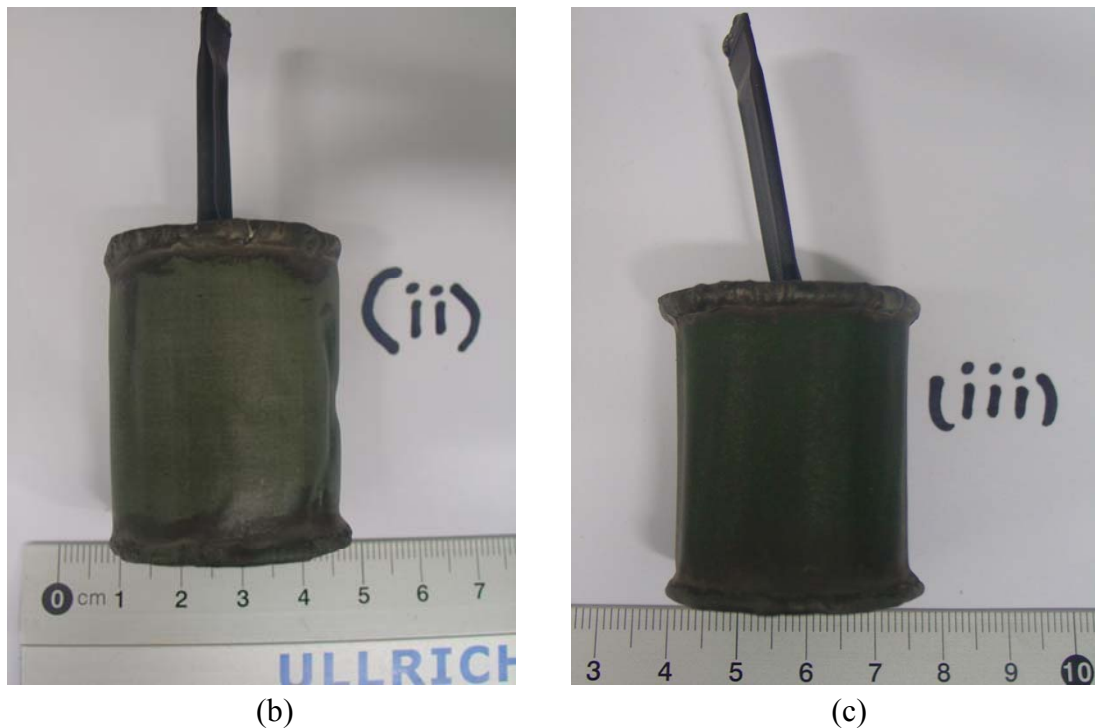
The relative density of Tax2 sample produced by Hipping was found to be 84% and the shrinkage of the canned sample after hipping was uneven as can be seen from the Figure 3.7(b). The tube of the can is shranked and was flat but there is hardly any shrinkage on the sides of the can suggesting that there is still some air trapped inside This is likely because some air leaked into the container during the time after press-sealing and the tube and before welding the end of the tube. The porosity level of Tax2 hipped material was quite high and the size of the pores ranged from 2 to 25t μm as shown in Figure 3.8(b).The Tax3 canned sample uniformly shranked from all sides and the shrinkage was 6% in both diameter and in height as shown in Figure

Chapter 3: Results and Discussions

3.7(c) .The relative density of Tax3 sample produced after HIPping was about 93, which means that the porosity level was fairly high. The size of the pore ranged from 1 μm to 8 μm and the pores were distributed evenly throughout the material. The most of the dark phase and gray phases are concentrated along the boundaries of the white phases and are equiaxed.



(a)



(b)

(c)

Figure 3.7: Consolidated samples produced by hot isostatic pressing of Titanox powders: (a) Tax1 (b) Tax2 (c) Tax3

Chapter 3: Results and Discussions

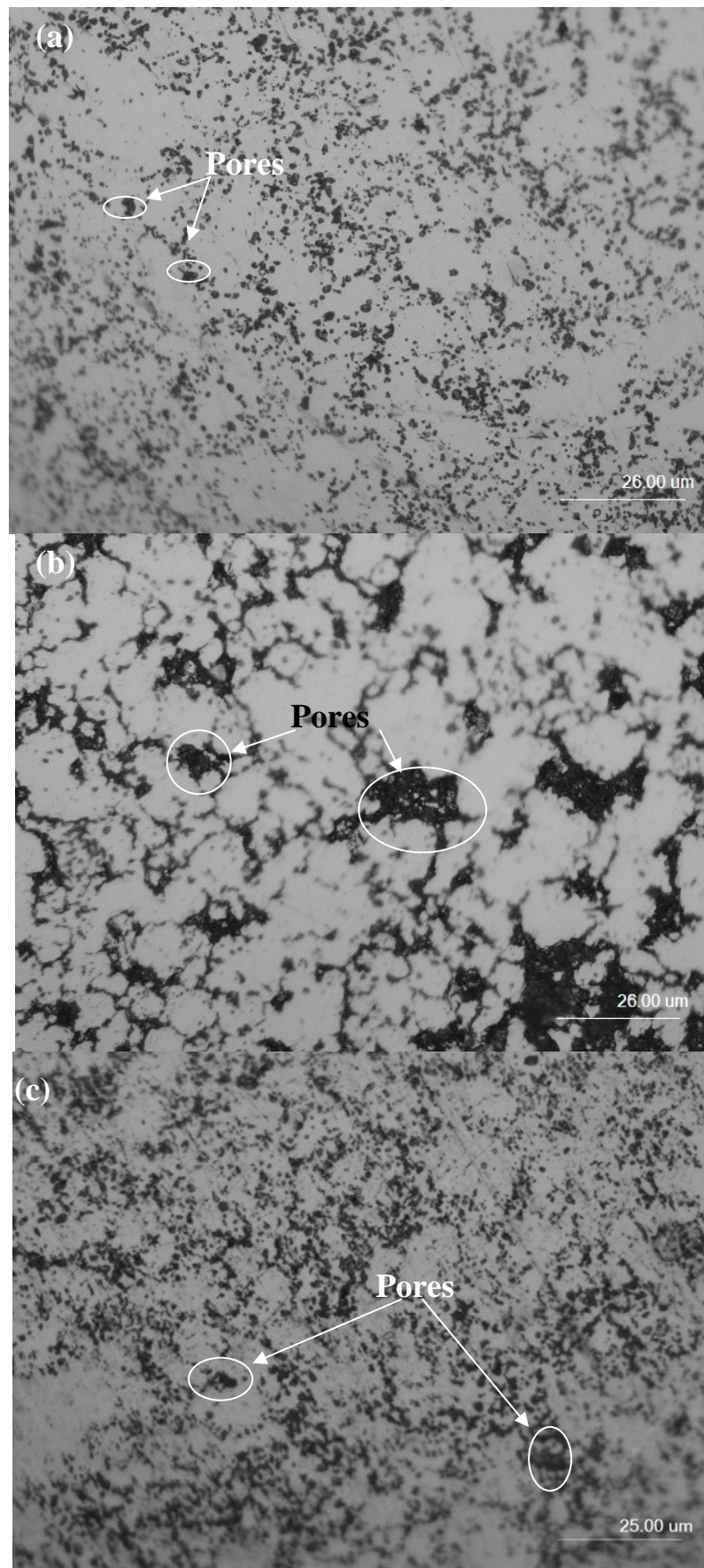


Figure 3.8: Optical micrograph of the hipped samples produced using Titanox powders (a) Tax 1(b) Tax2 (c) Tax3

3.3. Microstructures of the Hipped Samples Produced Using Titanox Powders

Figure 3.9 shows the XRD patterns of the consolidated samples produced by HIPping the three as-received Titanox powders at 1200°C under the pressure of 200MPA for two hours. The major phase in all the three consolidated samples was TiAl as shown by the well defined TiAl peaks of the XRD patterns in all the three consolidated samples compositions. A smaller fraction of α_2 -Ti₃Al phase and TiAl₃ was observed in Tax1 and Tax3 consolidated samples. XRD patterns also showed the presence of aluminium oxides in all the three hipped samples. This may be because of the high oxygen content in the as-received powders, and the oxygen combine with the aluminium during consolidation, resulting in the formation of aluminium oxide phase. For Tax2 consolidated sample, because of poor consolidation caused by the trapped gas and initial high oxygen content in the powders , Ti₂O formed besides Al₂O₃ during HIPping and this may suppress α_2 - Ti₃Al phase.

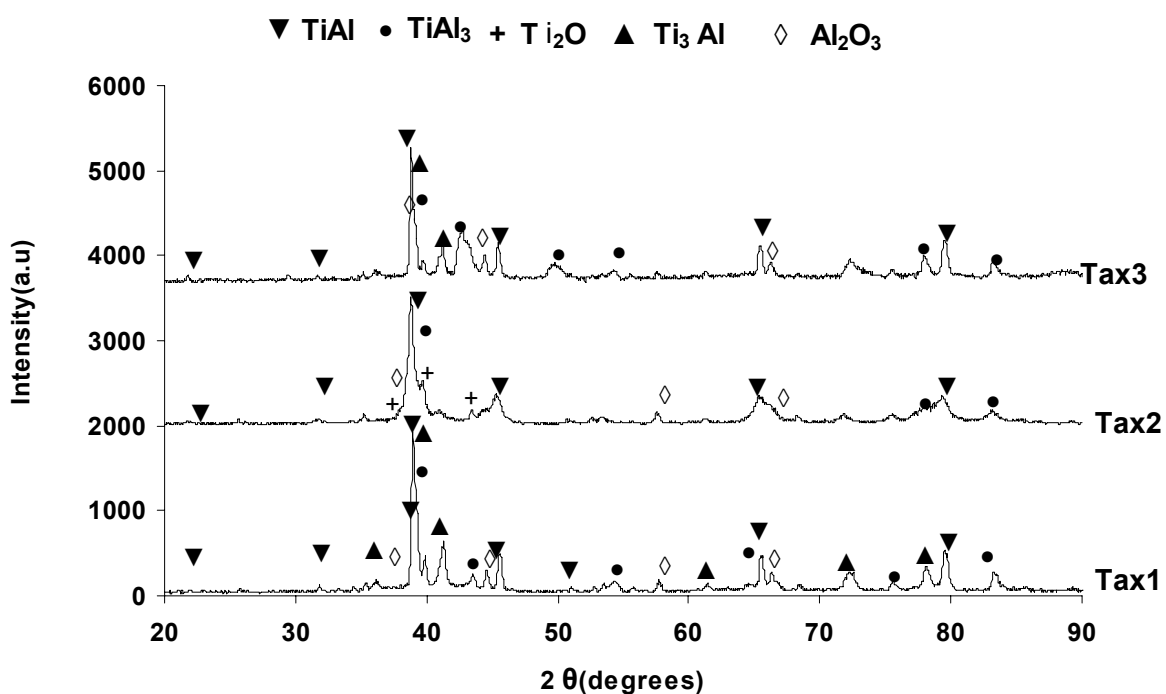


Figure 3.9 XRD Patterns of the consolidated samples produced by HIPping Titanox Powders Hipped at 1200°C

Chapter 3: Results and Discussions

Figure 3.10 shows secondary electron SEM image of the microstructures of the Tax1 HIPped sample and EDS spectra of from selected points on the microstructure. The dark particles as indicated by point 1 on the image Figure 3.10(a) have size in the range $0.7\mu\text{m}$ to $6\mu\text{m}$ and they are mainly distributed near the bright phase as indicated by point 3 on the image. Light grey phase denoted by point 2 on the image is the major continuous phase. EDS spectra from points 1-3 which are in the three different phases show the elements with the intensities. As shown in Figure 3.10(b) the particles of the dark phase (point 1) have very high aluminium content but very low titanium content. On the other end, bright phase and grey phase show high titanium content and slightly lower aluminium content .Figure 3.10(c) and (d) in the Tax1 HIPped sample contents. Table 3.2 shows the content of different elements in the different phases determined using semi-quantitative EDS analysis.

The content of aluminium in the dark phase is 45.1at% and that of Ti is 27.35at%. Oxygen content in the dark phase is extremely high 20.1at%, suggesting that dark particles are Al_2O_3 phases that was observed in the XRD pattern for Tax1 (Figure 3.9). A small amount of silicon and chromium was also observed in the composition analysis .The composition of grey phase appears to be homogeneous .At point 2 titanium content is 45.8at%.and that of aluminium is 47.8at%, oxygen content is 6.2at%. Again the composition analysis of the grey phase showed a small fraction of silicon and chromium. This suggests that the grey phase mainly consists of $\gamma -\text{TiAl}$ as determined by the XRD patterns. The bright phase is titanium rich and constitutes 54.4at% of titanium, 35.7at% aluminium and about 1.4at% of oxygen which is much lower compared to the other phases. The composition analysis also shows .3at% of silicon and .1at%of chromium. The titanium rich bright phase represents hexagonal $\alpha_2-\text{Ti}_3\text{Al}$ as supported by XRD.

Figure 3.11 show X-ray elemental maps of Tax1 hipped sample. As shown by the Figure 3.11 the distribution of aluminium and Titanium in the each phase is homogeneous. The X-ray elemental maps clearly shows that dark phase is aluminium rich(Figure3.11(b)) and the bright phase is titanium rich. The regions where the dark phase particles are concentrated also contains some pores as shown in Figure 3.10 as

Chapter 3: Results and Discussions

well Figure 3.8(a) As it can be seen in the Figure 3.10(a) distribution of the dark phase is uneven more concentrated near the bright phase.

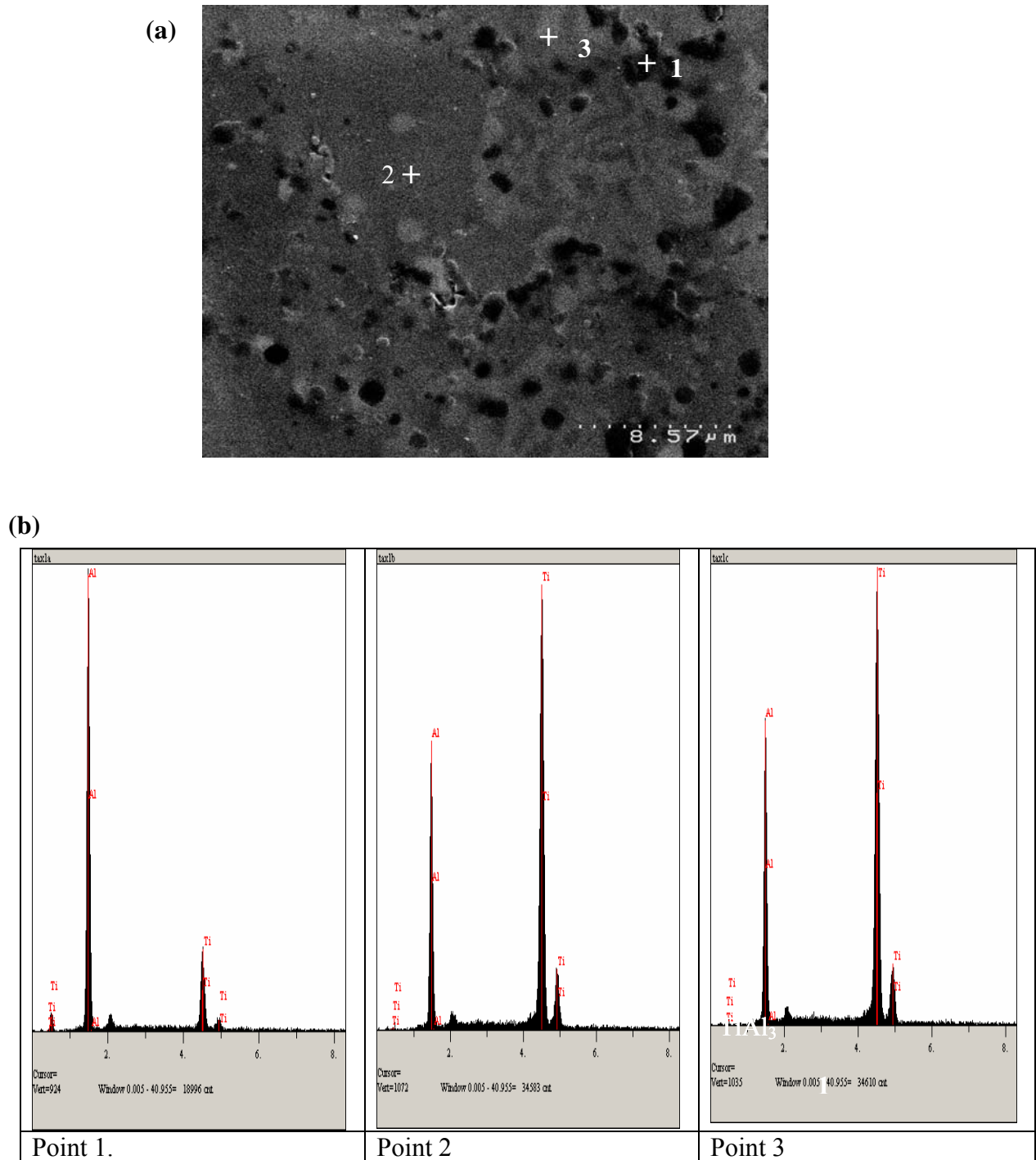


Figure 3.10: (a)SEM secondary electron image of sample;
(b) EDS spectra from points 1-3 shown on the image respectively

Chapter 3: Results and Discussions

Table 3.2: Content of different elements in (at%) in different phases determined using semi-quantitative EDS analysis of Tax1 hipped sample

Point	Ti	Al	O	Si	Cr
Point 1	27.4	45.1	20.1	0.1	0.2
Point 2	45.7	47.8	6.2	.1	.1
Point 3	54.4	35.7	1.4	0.3	.1

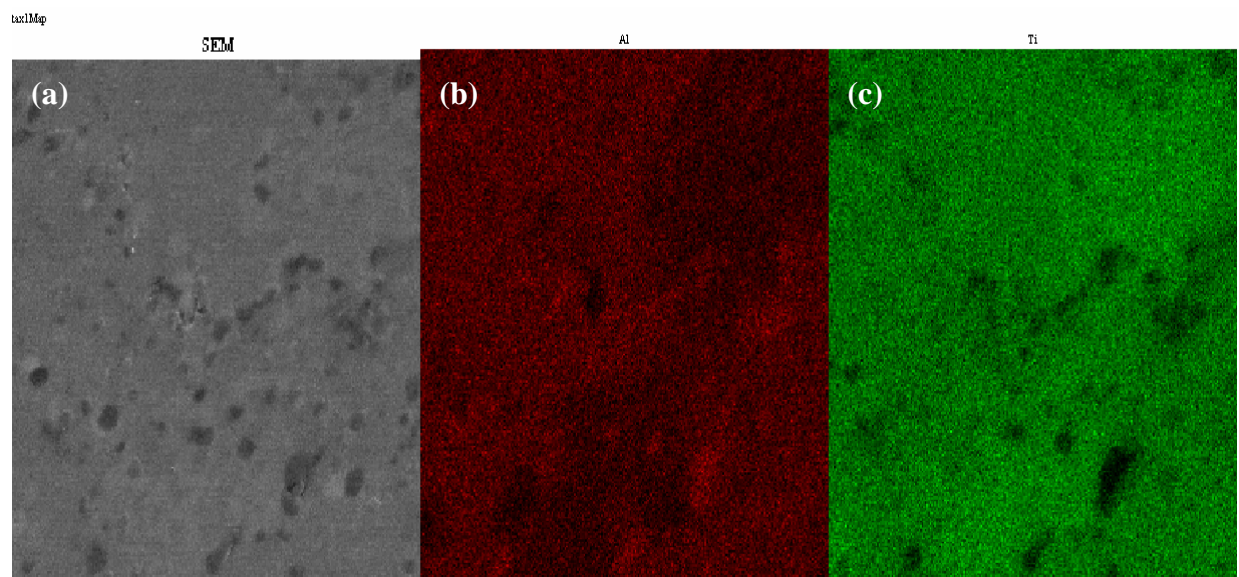


Figure 3.11: (a) SEM image and (b) and (c) X-ray elemental maps of Tax1 Hipped sample

Chapter 3: Results and Discussions

The SEM secondary electron image of the microstructure of Tax3 HIPped sample and EDS spectra from different selected points are shown in the Figure 3.12 and 3.13. The three different contrasts of the image represent particles of three different phases. Some pores adjacent to dark phase are noticeable. The particles of the dark phase have sizes the range of 0.5 to 4 μm , as denoted by point 1 on the image. The other two phases are grey and bright phase which are denoted by points 2 and 3 in Figure 3.12 respectively .

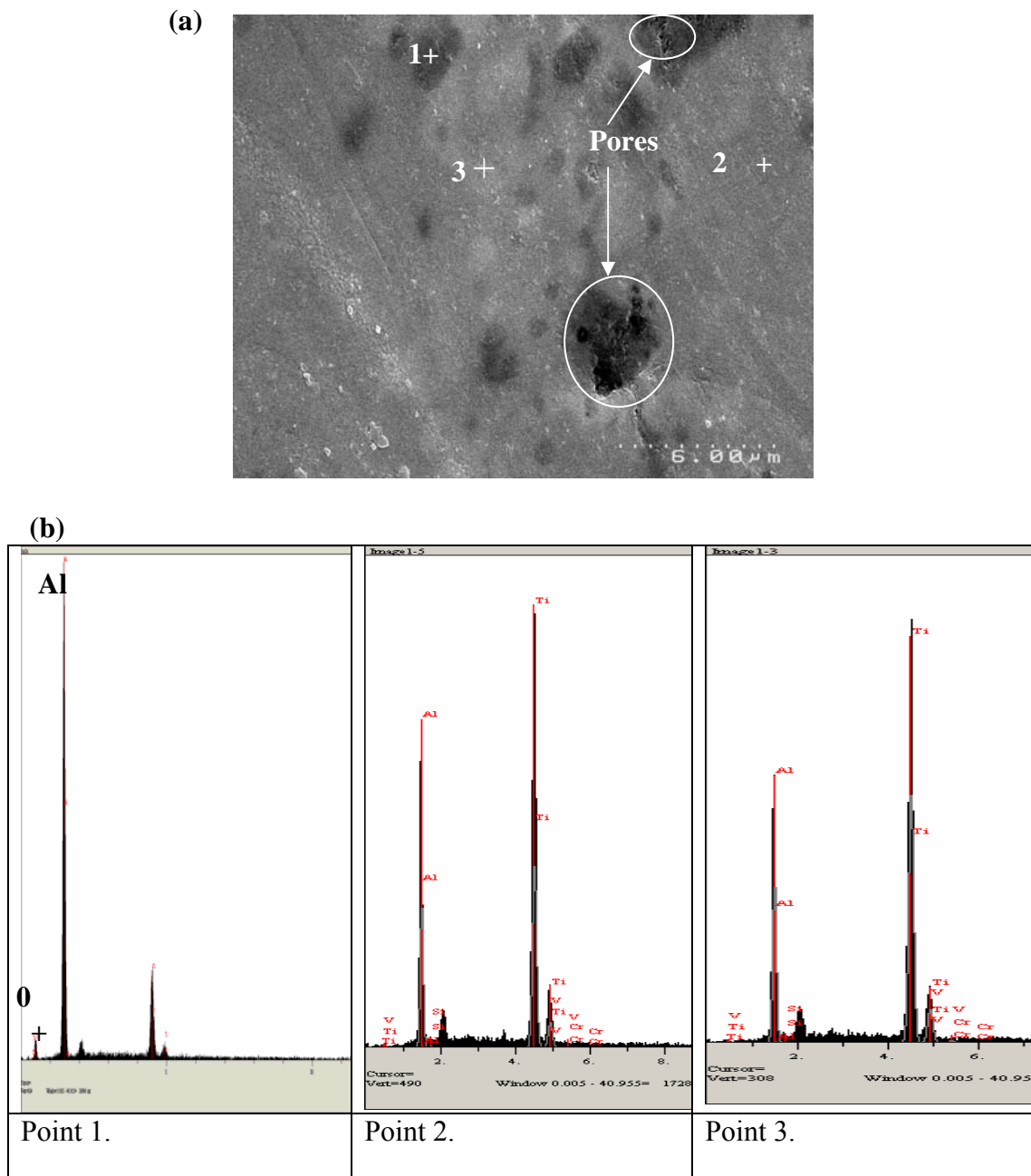


Figure 3.12: (a) SEM secondary electron image of the microstructure of Tax3 HIPPed sample and (b) EDS spectra from points 1-3 shown on the image, respectively

Chapter 3: Results and Discussions

The EDS spectra from points in different phases are shown in the Figure 3.12(b) The EDS spectrum from point 1 in the dark phase showed aluminium peak being the most intense peak followed by the titanium peak. An oxygen peak was also observed in the spectrum. The primary peaks of the EDS spectra from points 2 and 3 was titanium and aluminium spectrum. The content of the elements present in different phases determined by semi-quantitative analysis of the EDS spectrum from points 1-3 are shown in table 3.3 The dark phase denoted by point 1 is aluminium rich and has 54.9at% of aluminium and 30.5at% of titanium .The oxygen content in the dark phase is 14.4at% .The dark phase in the microstructure of Tax3 HIPped sample is likely a mixture of aluminium oxide Al_3Ti . Grey phase has homogeneous distribution of titanium and aluminium, is 49.9at% and 45.9at% titanium and aluminium content, confirming that the phase is TiAl phase. The oxygen content of the grey phase is 3.8at% and it has a small fraction of silicon and chromium. The bright phase in the microstructure of Tax3 HIPped sample has 50.5at% of titanium and 43.0at% of aluminium. Similar to that in the Tax1 HIPped sample the particles of the dark phase are more associated with the bright phase than grey TiAl phase.

Table 3.3: Concentration of different elements in different phases determined using semi-quantitative EDS analysis of Tax3 hipped sample

Point	Ti	Al	O	Si	Cr
Point 1	30.5	54.9	14.3	.08	.28
Point 2	49.9	45.9	3.8	.04	0.3
Point 3	50.5	43.0	6.1	0.8	0.2

3.4 Mechanical Behaviour of The Hipped Samples Produced Using Titanox Powders

The Figures 3.13 shows the engineering stress-engineering strain curves of tensile specimens from Tax1 HIPped samples tested at room temperature. Specimen 1 shows fracture strength of 123.6MPa which is considerably lower than the fracture strength of specimen 2which is 213MPa .The low fracture strength of the specimen might be because of premature breaking of the specimen 1near the grip section as shown in the Figure3.14 (a). The premature fracture of the specimen might be due to the pores in the material which are not uniformed distributed .On the other hand specimen 2 broke near the middle point of the specimen 2 as shown in Figure 3.14(b). There was no necking in any of the specimens tested at room temperatures and the stress strain curves of the tensile specimen. However yield stress of 185MPa was observed for specimen 1 of Tax1 at 900°C specimen 1 of Tax1 Figure 3.17 and specimen 2 of Tax3 at 800 °C showed some yield stress of 225 MPa Figure 3.18.

Engineering stress-strain curves of the tensile specimens from Tax1 HIPped samples tested at 800°C and 900° C are shown in the Figures 3.15 and 3.16 respectively. Specimen 1 showed the fracture strength of 213 MPa and specimen 2 showed highest fracture strength of 285MPa tested at 800°C.whereas relatively lower fracture strength of 201 and 193MPa was shown by the two specimens tested at 900°C. The two tensile specimens cut from Tax3 HIPped sample showed the fracture strength of 247 and 207MPa Figure 3.18. No necking was observed in any of the above specimens suggesting that the fractures for both Tax1 and Tax3 are brittle even at higher temperature.

The average values of the results obtained is shown in the table 3.4. Tax1 HIPped sample shows better strength than that of Tax3 HIPped sample at both room temperature at 800° C .Actually the room temperature fracture strength of Tax3 HIPped sample was found was significantly lower than that of Tax1. The slope calculated using stress- strain curves shows extremely lower values. For Tax1 and Tax3 at room temperature it is 5Gpa and 6GPa and at 800°C it is 6 and 7GPa and

Chapter 3: Results and Discussions

doesn't agree, even in the order of magnitude, modulus of TiAl. The possible reason can be that the amount of material deformation outside of the gauge length which has not been accounted for in the calculating the strain is significant and that the grips slipped relatively to the grip section of the specimen due to the deformation of the material in those sections

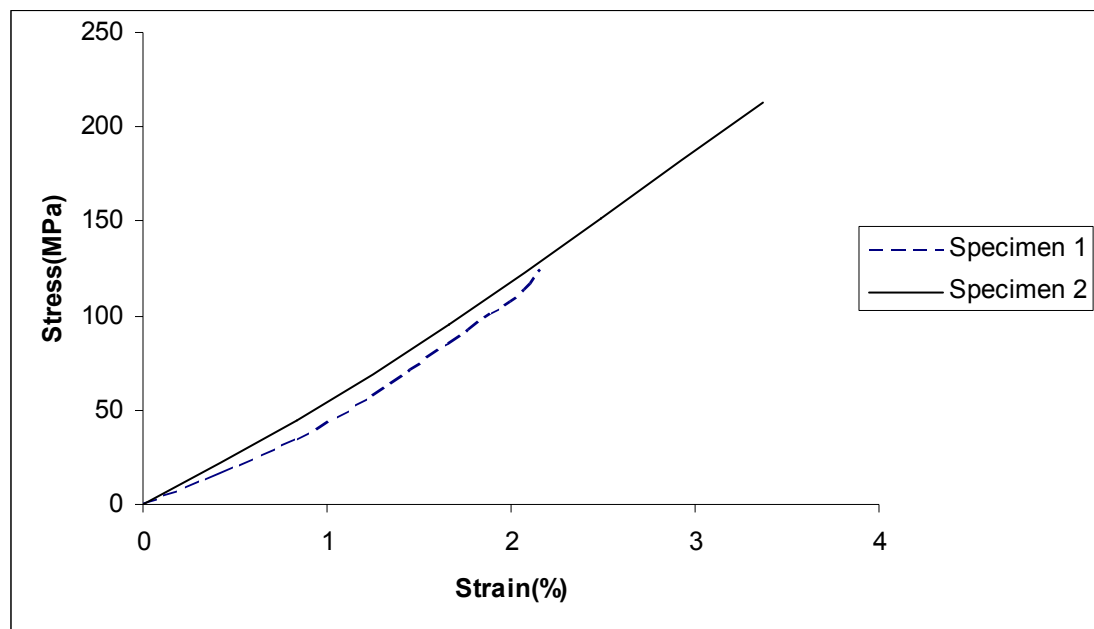


Figure 3.13: Stress vs Strain curves of specimens from Tax1 HIPped sample tested at room temperature



Figure 3.14: Broken Tensile specimens of Tax1 tested at room temperature
(a) specimen 1 (b) specimen 2

Chapter 3: Results and Discussions

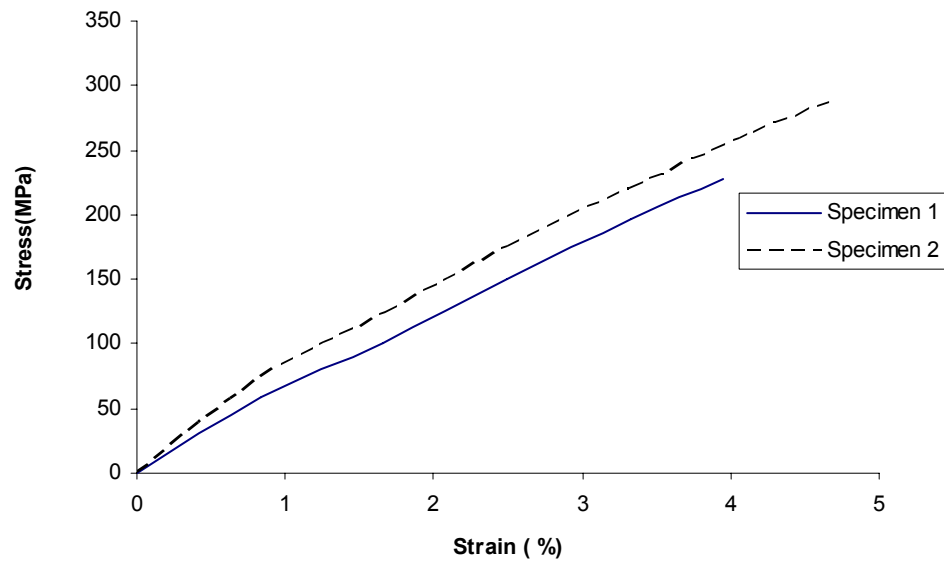


Figure 3.15: Stress vs Strain curves of specimens from Tax1 HIPped sample tested at 800° C

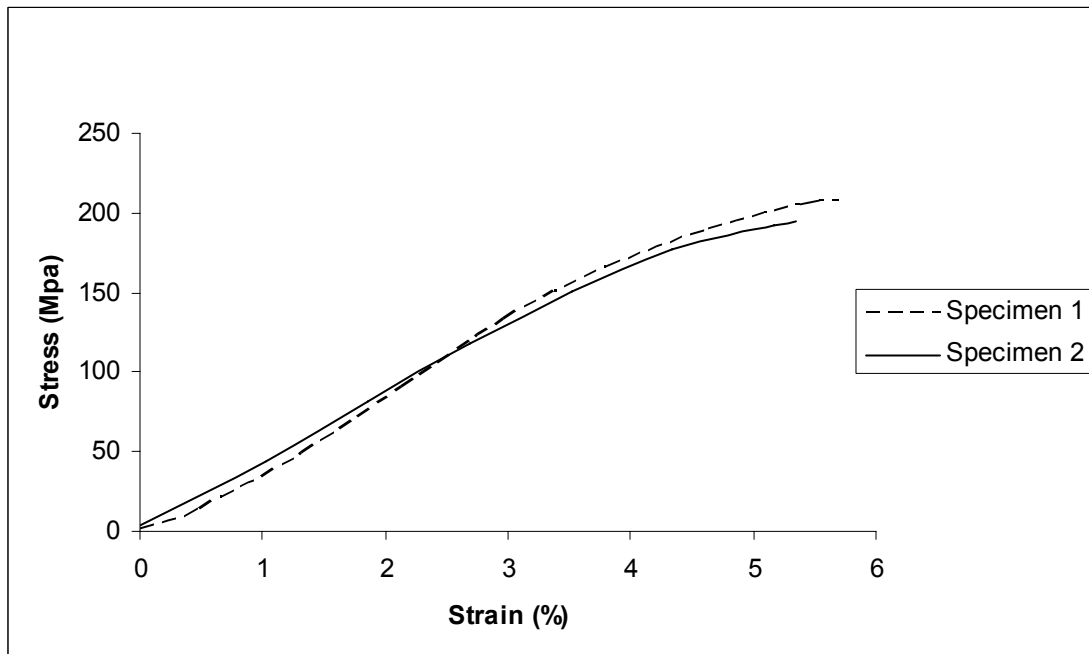


Figure 3.16: Stress vs Strain curves of specimen from Tax1 HIPped sample tested at 900° C

Chapter 3: Results and Discussions

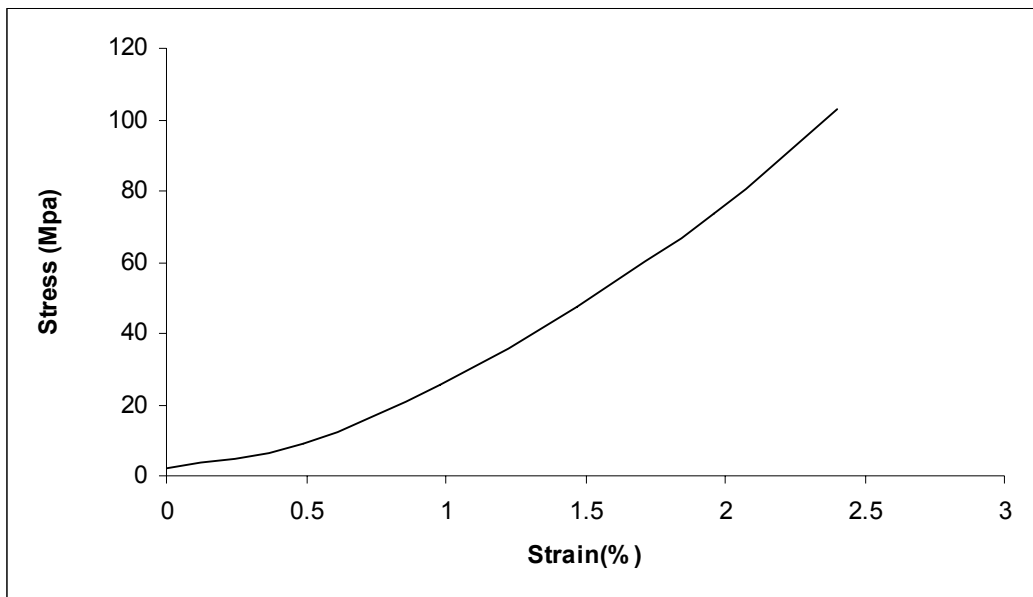


Figure 3.17 : Stress vs Strain curves of a specimen from Tax3 HIPped sample tested at room temperature

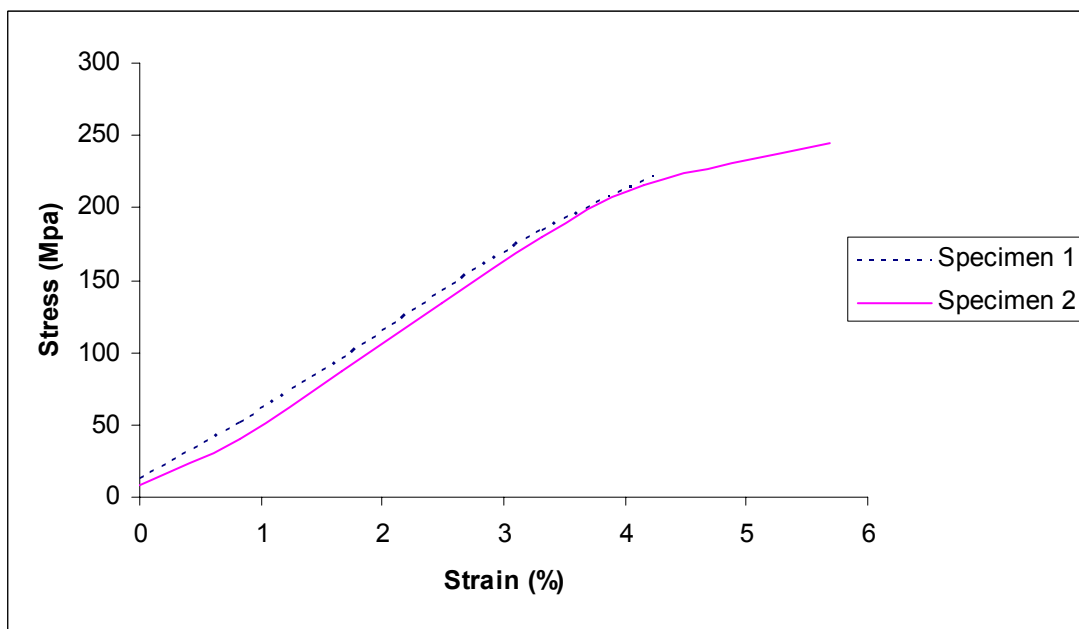


Figure 3.18: Stress vs Strain curves of specimens from Tax3 HIPped sample tested at 800°C

Chapter 3: Results and Discussions

Table 3.4: Fracture strength of Tax1 and Tax3 HIPped samples at different temperatures.

Material	Room - Temperature	800°C	900°C
Tax1	204	256	197
Tax3	103	234	n/a

Microhardness testing conducted on the HIPped samples using 25 grams of load and 20 seconds of loading duration shows the following results. The average microhardness of Tax1 and Tax3 HIPped samples found to be 596 HV and 610HV respectively. For both Tax1 and Tax 2 HIPped, samples the microhardness of the lighter phase region was lower than that of darker phase region. For Tax1 HIPped sample the average microhardness of the light and dark phase regions 501 ± 43 HV and 691 ± 90 HV respectively. The average microhardness of light and dark phases region in Tax3 HIPped sample was found to be 533 ± 54 HV and 688 ± 89 HV respectively. The Al rich dark phase region is harder than Ti rich light phase. This is likely because of the presence of hard phases like Al_2O_3 and TiAl_3 phase in the dark phase regions

3.5 Forging of the Tax2 Hipped Sample

Half of the Tax2 HIPped sample was canned as shown in Figure 3.19(a) and heated to 1160°C . The canned sample was then subjected to open die hammer forging with a high strain rate. The height of the canned sample was reduced from 21mm to 6.2mm leading to reduction of about 66%, increase in diameter was from 40mm to 58 mm leading to a pancake shape of the sample without cracking of the sample, as shown in Figure 3.19 (b and c). Examination of the microstructure of the forged sample showed that there was considerable reduction the volume fraction and sizes of the pores after

Chapter 3: Results and Discussions

forging as shown in the Figure 3.20. The relative density of the Tax2 HIPped sample was increased from 86% increased to 93% after forging. There was some chipping of the materials during cutting of the tensile specimen from the forged disk and some cracks were also formed on the specimen as shown in Figure 3.21

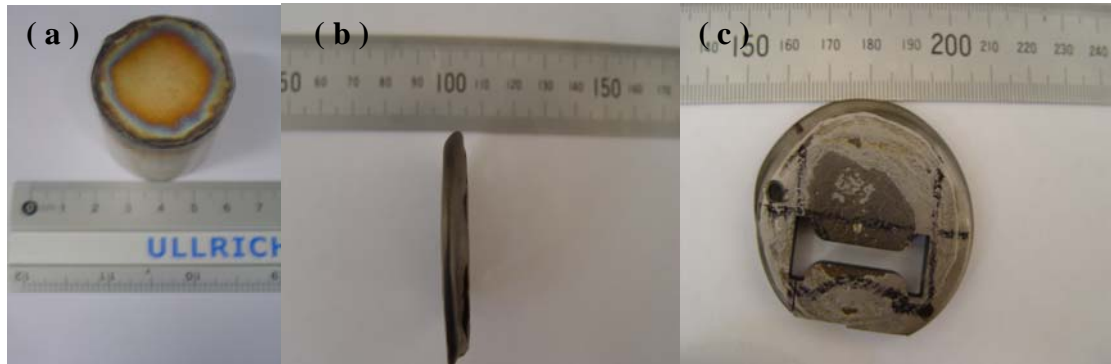


Figure 3.19: (a) Hipped Tax2 concealed by stainless steel can before Forging

- (a) Side view of the disk produced by forging of the consolidated sample
- (c) Planar view of the disk

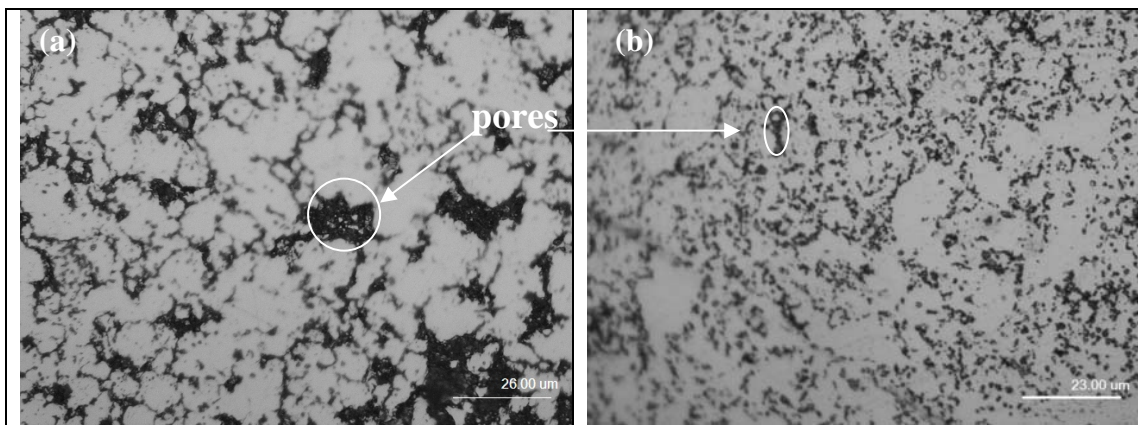


Figure 3.20 :Optical micrograph of Tax2 (a) HIPped at 1200°C

- (b) HIPped and Forged at 1200°C

Chapter 3: Results and Discussions

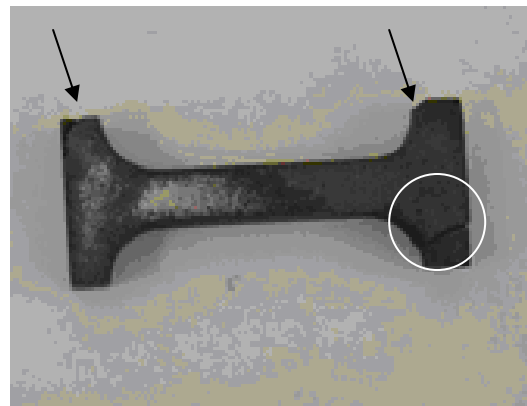


Figure 3.21: Cracks on the tensile specimen cut from the Tax2 forged disk

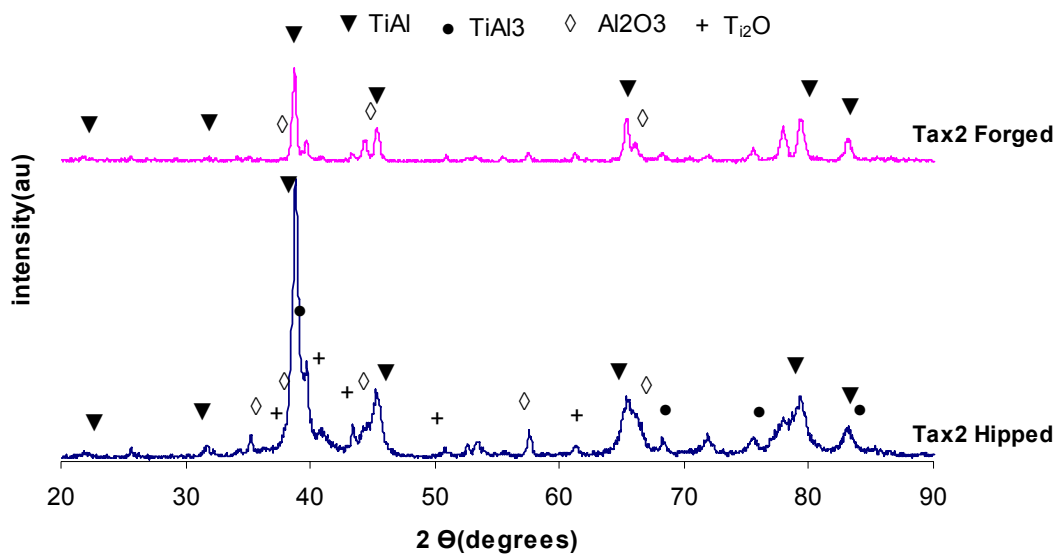


Figure 3.22: XRD Patterns of Tax2 Hipped sample before and after Forging

The white region on the surface of the tensile specimen is alumina. The alumina was used as a release agent and was put in the can before sealing .The intention of filling the gap between the HIPped sample and the can with alumina powder was to allow the can material and the HIPped sample to be deformed together minimize the possibility of oxidation during forging. The fracture strength of one specimen cut

Chapter 3: Results and Discussions

from the forged sample tested at room temperature was found to be 91MPa which was considerably lower than that of the tax1 Hipped sample tested at room temperature .This might be due to the micro-cracks introduced forging. The average microhardness of the forged sample was found to be 569 ± 40 Hv which is remarkably higher than the average microhardness of Tax2 which is 262HV from 262Hv which was of the hipped sample

XRD patterns of Tax2 HIPped sample before and after forging (Figure 3.22) show slight phase change occurred as a result of the hot forging. The TiAl peaks become sharper after forging suggesting that the grains grew larger during heating. TiAl_3 and Ti_2O phase disappeared suggesting that the two phases were dissolved or reacted during heating and forging .Figure 3.23 shows the microstructure of Tax2 HIPped sample after the hot forging. There is directional elongation of the bright and dark phase regions and the elongation is perpendicular to the forging direction.

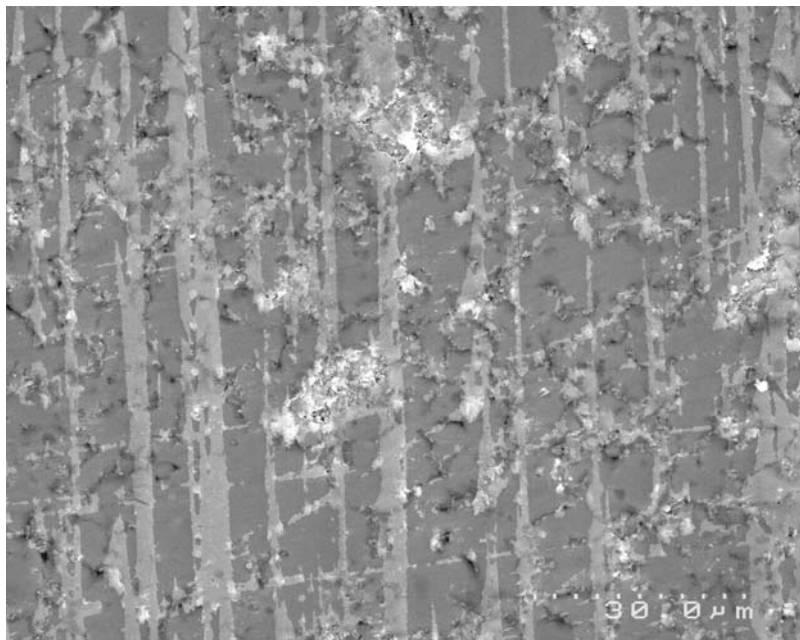


Figure 3.23: SEM secondary electron image of Tax2 HIPped sample after forging

Figure 3.24(b) shows another image of the forged sample taken at a high magnification, and Figure 3.24(b) shows EDS spectrum from three selected points in different regions shown in Figure 3.24(a). Similar to what was observed in Tax1 and Tax3 Hipped samples ,the dark phase contain high level of oxygen . So these phases which are concentrated at the periphery of other phases may contain aluminium

Chapter 3: Results and Discussions

oxides as indicated by XRD patterns. The light and the bright phases show approximately similar composition and have TiAl phases as confirmed by XRD patterns.

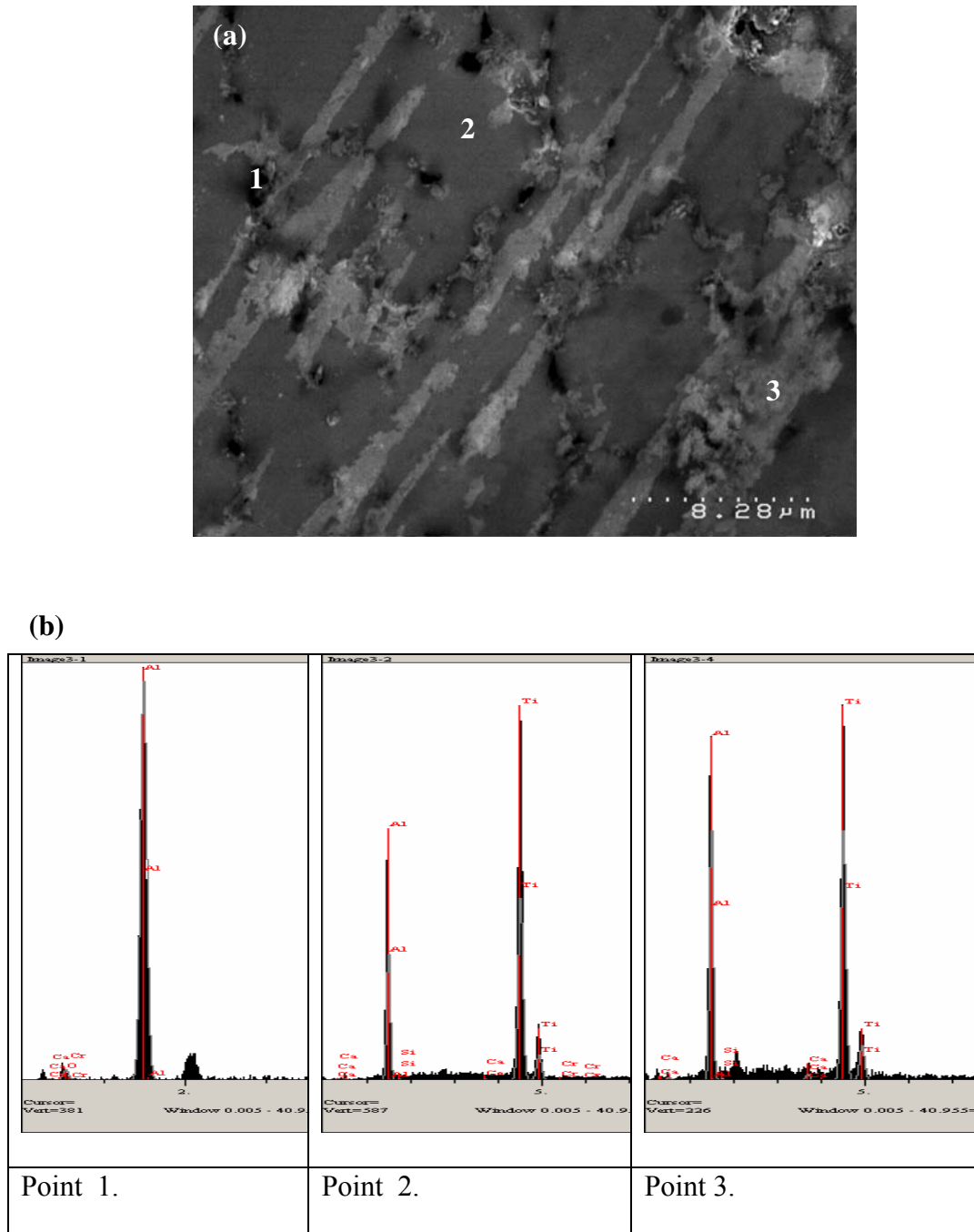


Figure 3.24: (a) SEM secondary image of Tax2 HIPped sample after hot forging(b)EDS spectra from point 1-3 shown in (a) respectively

3.6 Fracture Behaviour of the Tensile Testing Specimens

Figure 3.25 show the image of the broken tensile testing specimens from Tax1 HIPped sample. The specimen broke at the centre, the specimen again was broken close to the centre and the specimen was broken near the end. Figure 3.36-3.28 show the SEM images of the fractured surfaces of the tensile testing specimens from Tax1 at room temperature, 800°C and 900°C respectively. Cleavage type of brittle transgranular fracture was observed from the fractured surface of the specimen tested at room temperature. The fracture surface of the specimen tested at 800°C did not show clear cleavage type transgranular facets suggesting that fracture is ductile type of fracture in nature. The fracture surface of the specimen tested at 900°C shows fibrous morphology which may be due to the oxidation of the material. Surface oxidation for the specimens tested at 800° c and 900°C is observed as the colour of the samples after high temperature tensile tests become pale.

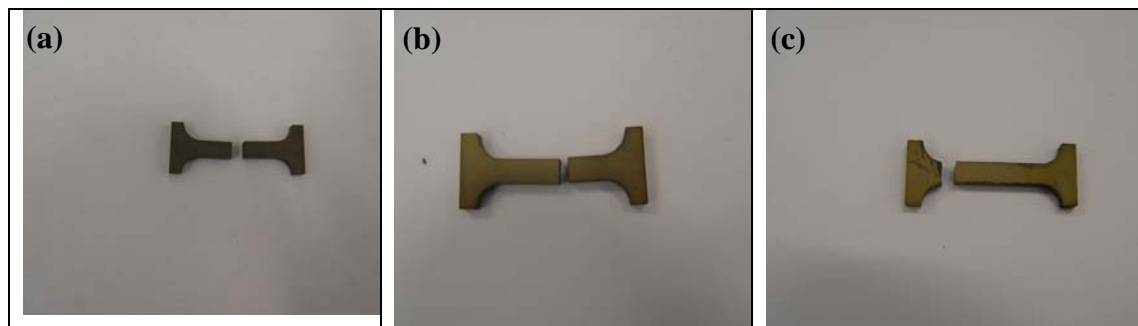


Figure 3.25: Broken tensile specimens from Tax1 HIPped sample tested at (a) room temperature (b) 800°C and (c) 900°C

Chapter 3: Results and Discussions

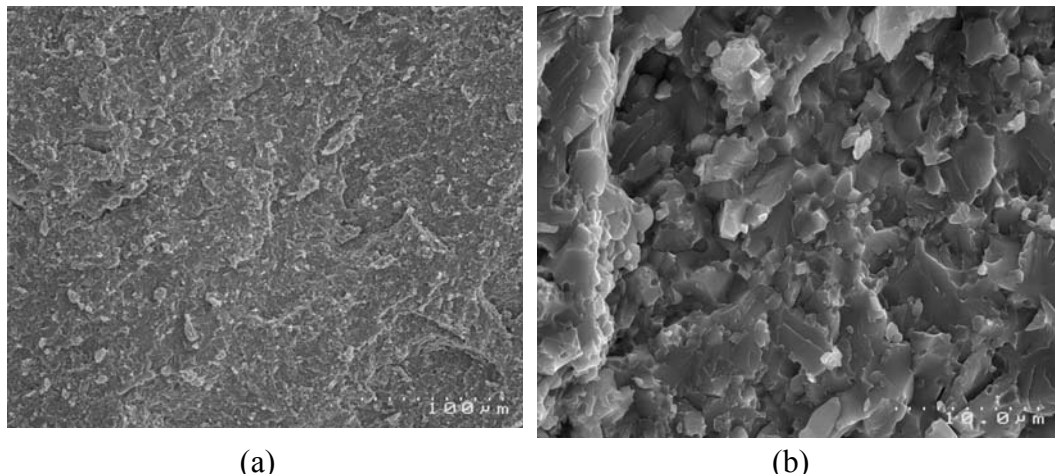


Figure 3.26: SEM secondary electron images of the fractured surface of tensile testing specimen for Tax1 HIPped sample tested at room temperature

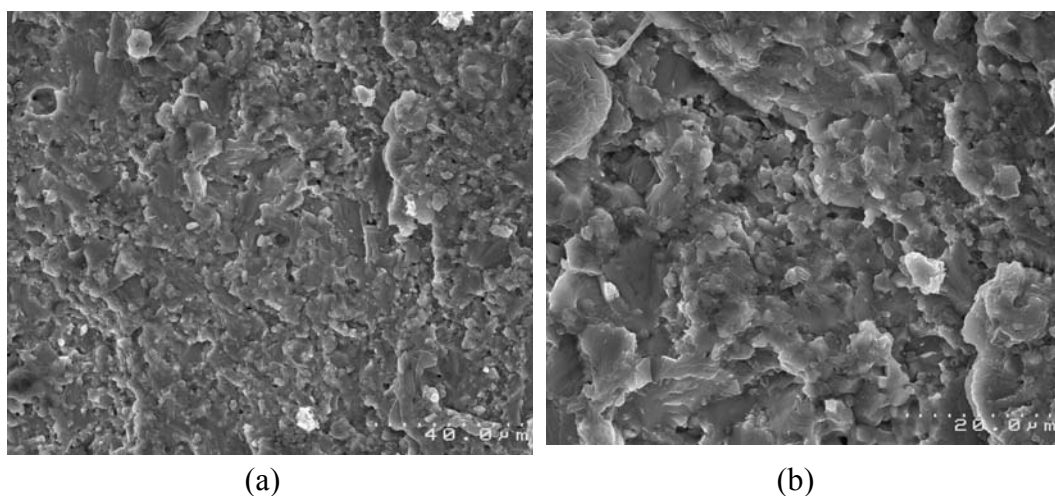


Figure 3.27: SEM secondary electron images of the fractured surface of tensile testing specimen for Tax1 HIPped sample tested at 800°C

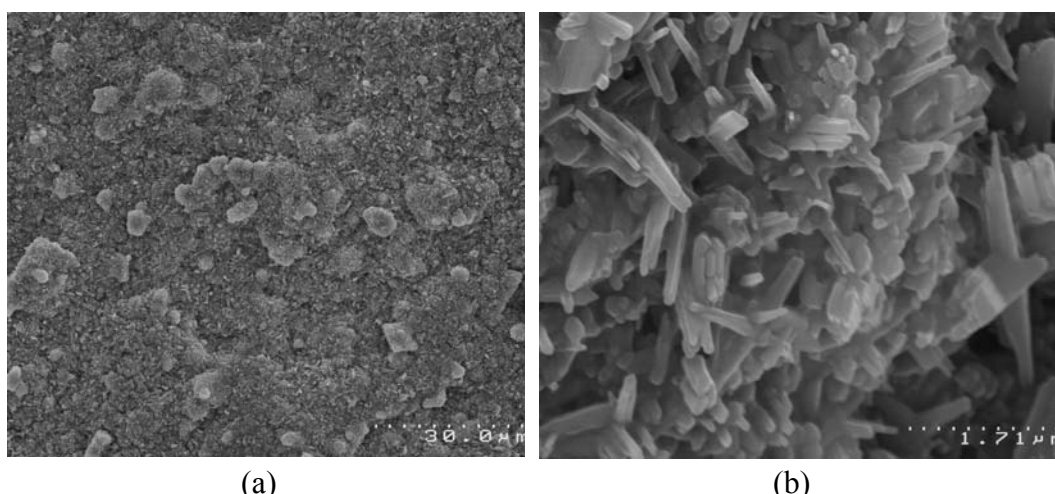


Figure 3.28: SEM secondary electron images of the fractured surface of tensile testing specimen for Tax1 HIPped sample tested at 900°C

3.7 Discussion

Diffusion in metals and alloys are mainly activated by the sintering temperature. The single phase TiAl powders results in different phases upon heating beyond $\alpha + \gamma$ transus temperature (1120°C)[4]. The major phase transformation from γ TiAl to titanium rich brighter α_2 . Ti_3Al phase and aluminium rich dark $TiAl_3$ are visible in all the three consolidated samples produced from the Titanox powders by hot isostatic pressing. Besides these major phase changes, presence of relatively high content of oxygen in all the three Titanox powders which plays major role in controlling the mechanical process and the mechanical properties of the consolidated samples. Titanium has great affinity towards oxygen and since the powder particle size is extremely small, and each powder particle is encapsulated by oxide layer [3], there is significant oxygen present even after the degassing process. So during hiping this oxygen gets dissolved and not surprisingly it leads to the formation of Al_2O_3 , TiO_2 and TiO . These oxides are detrimental to the material strength and the tensile properties [2]. This is the reason why the material strength is far too low and also couldn't achieve the required ductility even at elevated temperatures. Due to the high oxygen content, the hardness of the powder particle is very high even at high temperature. So even at high hipping temperature, so even at high HIPping temperature of 1200°C the TiAl powder particles cannot be effectively deformed and are unable to diffuse resulting in pores.

Compound often contains amount of residual porosity arises from the green compact ,pores due to kirkendall effect , porosity associated with gas evolution due to volatilization and molar volume defects due to intrinsic differences in the density and the reactants. Therefore pressure must be applied in some form during reactive sintering to synthesize and densify the product simultaneously. The applied pressure during hiping results in the closure of the pores. The application of high inert gas pressures and elevated temperatures results in the removal of internal voids and creates a strong bond throughout the material [3].

The application of isostatic pressure (200MPa) in the current research results in the 97% density for Tax1 and 93% for Tax3. For Tax2 poor consolidation and high porosity resulted due to the air leakage into the can during press seal and before

Chapter 3: Results and Discussions

welding the end of the tube. γ -TiAl is the major phase in all the three consolidated samples. However there were some fraction of α_2 -Ti₃Al and TiAl₃ phases present in Tax1 and Tax3 . The volume fractions of γ -TiAl and α_2 -Ti₃Al control the material strength and toughness [1, 3]. But it is the high oxygen content in the powders that eventually combined with aluminium in the HIPping process leads to the formation of Al₂O₃, in all the three HIPped materials not only led to weak inter-particle bonding causing low strength but also caused embrittlement and mainly responsible for premature breakage and transgranular cleavage type fracture even at high temperature. High porosity and oxidation of the tensile specimens conducted at higher temperature are other factors responsible for the low tensile strength.

There was some error while conducting tensile tests of the specimens. There was disproportion between the applied load and extension while conducting tests. The testing specimen tensile holder, dimension of the tensile specimens needs to be reviewed and investigated as the stress-strain curves showed some noticeable error.

References

1. F.Appel, R.Wagner “Microstructure and deformation of two phase γ - titanium aluminide “Material Science and Engineering R22 (1998) 187- 268.
2. M.Lamirand,J.I.Bonnentian,G.Ferriere,S.Guerin J.P. Chevalier “Relative effects of chromium and niobium on microstructure and properties as a function of oxygen content in TiAl alloys” scripta materiala,vol.(56) (5) (2007) p.325
3. V. Viswanathan, T. Laha, K. Balani, A. Agarwal and S. Seal “Challenges and advances in nanocomposite processing techniques” Materials Science and Engineering: R: Reports, Volume 54, Issues 5-6, 30 November 2006, Pages 121-285
4. Y. Mishin and Chr. Herzog “Diffusion in the Ti-Al system” Acta Materialia, Volume 48, Issue 3, 2 February 2000, Pages 589-623

Chapter 4:

Conclusions

and

Recommendations

4.1 Conclusions

- Characterization of three TiAl based powders of similar compositions produced by Titanox Development Ltd. has been done. Particle morphology and particle size distribution of the three powders from Titanox Development Ltd shows that the average particle size of the all the three powders are The particle size varies from $2\mu\text{m}$ to $25\mu\text{m}$ for Tax1 powder, $1\mu\text{m}$ to $5\mu\text{m}$ for Tax2 powder and from $0.5\mu\text{m}$ to $20\mu\text{m}$ for Tax3. The shape of the powder particle is irregular and generally equiaxed and the powder particle consists of single phase. XRD patterns showed predominate TiAl phase in all the three compositions of the powders.
- The chemical analysis of the powders found the oxygen content and was found that oxygen content in all the three powders were remarkably high. The oxygen content by weight percent in Tax1, Tax2, and Tax3 respectively was found to be 1.7, 2.5 and 3.1.
- Bulk samples from the three different powders of Titanox were produced using hot isostatic pressing at 1200°C under pressure of 200MPa for two hours. The relative density of the bulk samples Tax1, Tax2 and Tax3 were found to be 96%, 84% and 93%. Tax2 powder resulted into comparatively poor consolidation because some air leaked into the can during the time after press-sealing the tube and before welding the end of the tube Tax2. Tax2 forged sample subsequently underwent forging at 1160°C which increased its relative density to 93%.
- XRD patterns showed the predominate γ -TiAl phase in all the three Hipped samples, while small fractions of α_2 - Ti_3Al and TiAl_3 phases were observed in Tax1 and Tax3 in Hipped samples. There was presence of Al_2O_3 phase in all the three consolidated samples, resulted from combining of aluminium with the oxygen which was quite high in the as received powders.

- Tensile specimen for Tax1 HIPped material average tensile strength of 204 MPa ,256MPa and 186MPa tested at room temperature ,800°C and 900°C respectively, while Tax3 material respectively showed average tensile strength of 103MPa and 234MPa at room temperature and 800°C temperature. The fracture observed was transgranular cleavage type brittle fracture for all the specimens at all temperatures. The embrittlement is due to Al_2O_3 formed during HIPping and also due to the high porosity level in the materials.

Recommendations for Future Work

- The high oxygen content of the Titanox powders is the key issue. Powder preparation method has to be improved in order to achieve quality material. The size of the powder particle of all the three compositions is too small which it self increase oxygen content. As surface particle is encapsulated by oxygen layer and hence increases the total oxygen volume.
- Present Press sealing process is not 100% reliable. Degassing process has to be improved. In the present process there is possibility of gas leakage into the can during press seal and before welding the tube after pressing and thus deteriorates the quality of degassing. Knife edge spot welder can be the good option can eliminate the possibility of any leaking .
- There was some an error in the tensile testing procedure specially when the specimens were tested at high temperature. The tensile testing fixture and dimensions of the tensile specimens need to be reviewed for better results.
- There was oxidation of tensile specimens while being tested at 800°C and 900°C. There is need for a proper control chamber for testing specimen at higher temperature